Screening of synthesis conditions for the development of a radium ionimprinted polymer using the dummy template imprinting approach

Marine Boudias, Sofiane Korchi, Alkiviadis Gourgiotis, Audrey Combès, Charlotte Cazala, Valérie Pichon, Nathalie Delaunay

Screening of synthesis conditions for the development of a radium ion-imprinted polymer using the dummy template imprinting approach

Marine Boudias[a,b], Sofiane Korchi[a,b], Alkiviadis Gourgiotis[b], Audrey Combès[a], Charlotte Cazala[b], Valérie Pichon[a,c], Nathalie Delaunay[a,*]

[a]*Department of Analytical, Bioanalytical Sciences, and Miniaturization, UMR 8231 Chemistry, Biology and Innovation, ESPCI Paris, PSL University, CNRS, 10 rue Vauquelin 75005 Paris, France*
[b]*Institut de Radioprotection et de Sûreté Nucléaire (IRSN), PSE-ENV/SEDRE/LELI, Fontenay-aux-Roses, 92260, France*
[c]*Sorbonne Université, 75005 Paris, France*

[*]Corresponding author at: Laboratoire des Sciences Analytiques, Bioanalytiques et miniaturisation – UMR 8231 Chimie Biologie Innovation, CNRS - ESPCI Paris PSL, 75005 Paris, France; E-mail address: nathalie.delaunay@espci.fr (Nathalie Delaunay).

Abstract

In this study, a selective and specific sorbent for radium extraction was developed for the first time using ion-imprinted polymer technology. A novel and original approach was used in order to screen the best synthesis conditions. After identifying the best monomer candidates, porogen, and complexation time from electrospray ionization mass spectrometry experiments, solubility tests, and conductimetry experiments, five ion-imprinted polymers (IIPs) were synthesized by bulk polymerization using Ba^{2+} as a dummy template ion. Non-imprinted polymers (NIPs) were similarly prepared but without template ions. Polymers were packed in solid phase extraction (SPE) cartridges for their characterization. Composition of the percolation and washing solutions (e.g. buffer concentration, nature and pH, and ethanol proportion) was varied to achieve the highest retention for the template ion while minimizing that of interfering ions. The retention, selectivity (retention on IIP *versus* on NIP), and specificity (targeted ions *versus* interfering ions) properties of the different polymers were compared by measuring the recovery yields in the SPE collected fractions by inductively coupled plasma mass spectrometry (ICP-MS). The IIP synthesized in acetonitrile/dimethylsulfoxyde (1/1, v/v) using Ba^{2+} as template ion, vinylphosphonic acid as complexing monomer, and styrene and divinylbenzene as co-monomer and cross-linker showed both selectivity and specificity. It retained strongly Ra^{2+} while having the potential to isolate it from alkali metals, metalloids and some transition metals.

Keywords

Specific extraction, Ion-imprinted polymer, Barium, Radium, Solid phase extraction, ICP-MS

Abbreviations

2-VP: 2-vinylpyridine; ACN: Acetonitrile; AIBN: Azo-N,N'-diisobutyronitrile; BET: Brunauer-Emmet-Teller; Bis-Tris: 2-[Bis(2-hydroxyethyl)amino]-2-(hydroxymethyl)propane-1,3-diol; CN: Coordination number; DEGDE: Di(ethylene glycol) divinyl ether; DMSO: Dimethylsulfoxyde; dSPE: Dispersive solid phase extraction; DVB: Divinylbenzene; EGDMA: Ethylene glycol dimethacrylate; EIC: Extracted ion chromatogram; ESI: Electrospray ionization; FTIR: Fourier transform infrared spectroscopy; ICP-(CC)-Q-MS: ICP-MS with a collision reaction cell; ICP-MS: Inductively coupled plasma mass spectrometry; ICP-QQQ-MS: Triple quadrupole ICP-MS; IIP: Ion-imprinted polymer; IS: Internal standard; LOQ: Limit of quantification; MAA: Methacrylic acid; MIP: Molecularly imprinted polymer; MS/MS: Tandem mass spectrometry; NIP: Non-imprinted polymer; RMN: Nuclear magnetic resonance; SPE: Solid phase extraction; TGA: Thermogravimetric analysis; UP: Ultrapure; VPA: Vinylphosphonic acid.

1. Introduction

Radium-226 is a natural radiotoxic radionuclide with a half-life of 1,600 years that is part of the uranium-238 decay chain. Its release to the environment is heightened by human activities such as uranium, coal, and phosphate mining, or shale gas extraction [1]. As radium shares similar properties with calcium, it can be involved in biological processes. In addition, during its decay, ^{226}Ra forms highly radioactive radon gas. Its persistence in the environment thus represents a risk of internal exposure to ionizing radiations for populations and ecosystems. For these reasons, radiological monitoring of the environment is a major concern. To date, there is still many grey areas regarding the processes of radium migration in the environment. This is due in part to the analytical challenge of accurately determining ultra-trace level of ^{226}Ra in complex environmental samples. A sample pretreatment step to concentrate it is therefore essential before analysis, independently of the measurement technique selected (mass spectrometry or radiometry).

Solid-phase extraction (SPE) is an efficient technique enabling to extract and purify analytes contained in complex samples. However, among commercial resins, rare succeed alone to selectively extract Ra^{2+} from the other alkali or alkaline-earth cations that are much more concentrated in the samples [2,3]. Most extraction procedures, followed by an ICP-MS analysis, employ the AG50W-X8 cation exchange resin alone [4–7] or in combination with a strontium specific resin (Sr resin) [8–14], jointly with complex and multi-steps protocols often including an evaporation step between the two resins. AnaLig® Ra-01 is the only Ra-specific resin available on the market but it is expensive, probably due to the cost of the synthesis of the macrocyclic ligand that it contains. Moreover, it requires the use of an organic complexing agent for Ra^{2+} elution which is not fully compatible with ICP-MS analysis depending on the introduction system employed [15,16]. The development of ion-imprinted polymers (IIPs) appears as an alternative to increase sorbent specificity and to allow Ra^{2+} elution with ICP-MS compatible solutions, and this at a much lower cost since they are most of the time prepared from commercial reagents.

Synthesized in the presence of the targeted ion or an analogous ion forming a complex with one or several kinds of monomers, after polymerization in the presence of a cross-linker and removal of the template ions, IIPs possess specific cavities, complementary in terms of size, shape, and functionalities to the targeted ion, enabling its specific recognition. A non-imprinted polymer (NIP) is also synthesized under the same conditions, but without the introduction of a template ion. It is, in theory, formed of ligands randomly organized and thus is used, as control sorbent, to demonstrate the imprinting effect. Since their appearance in the late 70's, development of IIPs as more specific sorbents for extraction in batch or in SPE cartridge, or sensors for heavy metals, transition metals, rare earths, and actinides, has largely gained in attractiveness [17–19]. Though IIPs has already been developed for other radionuclides [20], it has not been the case yet for radium extraction, which was the objective of the present study.

For radiological protection reasons and due to similar chemical properties, Ba^{2+} was selected as a Ra^{2+} analogue for the development of the IIPs. The use of an analogous ion is also advantageous as it prevents any radium contamination resulting from an incomplete elimination of the template during the forthcoming sample analysis. Ba^{2+} was considered a good candidate because it has a close hydrated ionic radius to that of Ra^{2+} (4.04 and 3.98 Å, respectively) [1] and also shares the same preferred coordination number (CN = 8) [21,22]. Synthesis conditions implemented for IIPs designed for other alkaline earth metals were first reviewed. However, very little literature on this subject was available. Only 12 articles focused on this topic, among them 10 were about strontium IIPs [23–32], 1 about a calcium IIP [33], and 1 about an IIP for alkaline earth metals (Mg^{2+}, Ca^{2+}, Sr^{2+}, and Ba^{2+}) [34]. Indeed, the interest and number of possible applications remain higher for heavy metals. Moreover, due to their low charge density, low electronegativity, and large ionic radius, they are less likely to form stable complexes with monomers than other ions.

Three approaches may be employed to elaborate an IIP (crosslinking of linear chain polymers, chemical immobilization of a monomer bearing a vinyl function, and trapping of a non-vinylated ligand), but strontium IIPs abovementioned were only synthesized using the first two methods [18]. However, the crosslinking approach does not offer a wide choice of commercial linear chain polymers and thus less chance to make a specific IIP and IIPs developed through the trapping approach may produce unrepeatable results due to the loss of the trapped ligand after several uses of the support [35]. Chemical immobilization was thus selected for this work in combination with bulk polymerization. Methacrylic acid (MAA) is the only vinylated monomer that has been used in this context [26,28,29]. Uncommon monomers (e.g. bis(trimethoxysilylpropyl)amine [25], dithiothreitol [34], and formaldehyde condensate [23]) capable of reacting with the cross-linker to form covalent bonds were also reported. 2-vinylpyridine (2-VP) and vinylphosphonic acid (VPA) have also proven their worth for other IIP syntheses [36,37] and phosphoric acid based-polydendate ligands are good chelating agents for alkaline-earth metals [38]. The lack of information provided in existing literature led us to establish a screening strategy to preselect synthesis conditions in a rational way instead of proceeding by trial and error as it is still often the case nowadays. The most critical step of an imprinted polymer synthesis corresponds to the complexation step between template and monomers. Computational simulations or spectroscopic methods (e.g. UV-vis, FTIR or RMN) have already been used to preselect the best monomers candidates and template/monomer ratio for molecular or ion-imprinted polymers synthesis [39–41]. However, carrying out theoretical calculations and reliable modelings require specific knowledge. Indeed, handling modeling softwares, selecting the right model and input data to be the most representative to the real system may be really complex for someone not familiar. Processing results of FTIR or RMN complexation studies may be time-consuming and depending on their structure, all monomers or complexes do not absorb UV or visible radiations. The use of experimental designs in combination with these techniques can also bring valuable information on key parameters governing the imprinting process but remains a laborious approach for IIPs prepared by the bulk method [39].

In this article, the affinity of several monomers for Ba^{2+} and the coordination of complexes were screened for the first time by electrospray ionization mass spectrometry (ESI-MS), a technique which is currently widely available in analytical chemistry laboratories and which provides rapid results. Formation of complexes in the synthesis solvent were further confirmed by conductimetry experiments. The IIPs/NIPs corresponding to the most promising conditions were then synthesized. Composition and/or volumes of the percolation, washing, and elution solutions were first optimized in order to evaluate the potential of the polymers for SPE. The quantification of the tested ions in each SPE fraction was carried out by inductively coupled plasma mass spectrometry (ICP-MS). Brunauer-Emmet-Teller (BET) surface areas of some IIPs and NIPs were also compared to correlate information brought by the extraction profiles. The most promising IIP in terms of both retention, selectivity, and specificity was finally evaluated for radium extraction in the presence of a wide range of interfering ions.

2. Material and methods

2.1. Reagents

Barium nitrate (99.999%), nickel nitrate hexahydrate (99.999%) and 2-[Bis(2-hydroxyethyl)amino]-2-(hydroxymethyl)propane-1,3-diol (Bis-Tris, ≥99%) were purchased from Sigma-Aldrich (Saint-Quentin-Fallavier, France) and VWR Chemicals (Fontenay-sous-Bois, France), respectively. Solvents, including HPLC-grade acetonitrile (ACN), HPLC-grade ethanol, and HPLC-grade methanol were provided by Carlo Erba (Val-de-Reuil, France), while anhydrous 2-methoxyethanol (99.8%), anhydrous dimethylsulfoxyde (DMSO, ≥99.9%), 2-VP (97%), di(ethylene glycol) divinyl ether (DEGDE, 99%), MAA (99%), VPA (97%), styrene (≥99%), and divinylbenzene (DVB, 80%) were purchased from Sigma-Aldrich. MAA was purified by vacuum distillation in order to remove the polymerization inhibitor, and stored at -20 °C. Azo-N,N'-diisobutyronitrile (AIBN) was provided by Acros Organics (Noisy-le-Grand, France).

High purity nitric acid was obtained by distillation (Savillex® DST-1000 system) from HNO_3 68% Normapur provided by VWR Chemicals. To prepare alkaline solutions, ammonia 25% Suprapur from Merck (Darmstadt, Germany) was used. Ultrapure (UP) water was produced using a Milli-Q system from Millipore (Molsheim, France). 1000 mg L^{-1} mono-elemental stock solutions of Ba in 2% HNO_3 (SPEX CertiPrep), of Cs in 2% HNO_3 (SPEX CertiPrep), of La in 2% HNO_3 (CPA Chem, Zagora, Bulgaria), of Th in 5% HNO_3 (Plasmanorm, VWR), of W in 5% HNO_3 (Alfa Aesar), and of Ni in 2-5% (BDH Aristar) were used. A multi-elemental solution of 33 elements, each at 100 mg L^{-1} in 5% HNO_3 (M33 containing Ag, Al, As, B, Ba, Be, Bi, Ca, Cd, Co, Cr, Cs, Cu, Fe, In, K, Li, Mg, Mn, Mo, Na, Ni, Nb, Pb, Rb, Sb, Se, Sr, Ti, Tl, V, U, and Zn) was obtained from CPA Chem. An in-house ^{226}Ra source with a specific activity of 11.92 Bq g^{-1} was used to prepare the percolation solution for the test on the target element of this study. For some experiments, Tl (*m/z* 205) was employed as internal standard at 0.1 µg L^{-1} (CPA Chem). All sample dilutions and solutions for ICP-MS analysis (calibration standards, blanks, and washing solutions) were performed with 0.5 mol L^{-1} (M) i.e. ∼3% HNO_3. When a calibration was used for quantification, concentrations of the ICP-MS standard solutions ranged from 0.01 (Cs) or 0.03 (Ba) to 10 µg L^{-1}.

2.2. ESI-MS experiments

Eight types of solutions corresponding to different ligands (DEGDE, MAA, 2-VP, and VPA respectively for the solutions A, B, C, and D) were prepared in MeOH/water (1/1, v/v). The solutions were prepared either in stoichiometric proportion (metal/ligand ratio (M/L) of 1/1 with 10^{-4} M of $Ba(NO_3)_2$) (solutions A–D) or with an excess of ligands (M/L of 1/6) (solutions A'–D'). Combinations of 2 ligands in ratio M/L1/L2 of 1/4/3 were also tested and led to the preparation of three additional solutions: mixture of DEGDE and MAA (solution E); mixture of DEGDE and 2-VP (solution F); and mixture of DEGDE and VPA (solution G).

Nature of complexes formed and kinetics of their formation were studied by infusion of the complexation solutions in ESI-MS with an Orbitrap Q Exactive Plus mass spectrometer (Thermo Fisher Scientific, Courtaboeuf, France), in both positive (ESI(+)) and negative (ESI(-)) modes. Mass calibration was performed weekly using Pierce LTQ Velos ESI positive ion calibration solution (*m/z* range: 138–1622) and Pierce LTQ Velos ESI negative ion calibration solution (*m/z* range: 265–1780) from Thermo Fisher Scientific. All data acquisition on the MS system was controlled by the Xcalibur 4.1 software. Source parameters were optimized in order to have the highest sensitivity while infusing solutions in the softest ionization conditions (relatively low gas flow rates and temperatures) so that complexes remain intact. The ESI source parameters were set as follows: sheath gas flow-rate, 10; auxiliary gas flow-rate, 1; spray voltage, 3 kV; capillary temperature, 120°C; S-lens RF level, 55; auxiliary gas heater temperature, 30°C. All solutions were infused at a flow rate of 10 µL min^{-1} after respectively a "short" and a "long" incubation time. Solutions with only one type of ligand (A–D and A'–D') were infused

after ~2 h and ~24 h. Solutions with two types of ligands (E–G) were infused ~2 h and ~24 h after addition of L2, itself being added ~24 h after addition of L1.
Data processing was performed with FreeStyle 1.3 software. The MS spectrum was registered in scan mode (*m/z* 60–900) at a resolution of 140,000 during 1 minute and an average mass spectrum was generated. A "home-made" database containing the theoretical *m/z* of the wide range of theoretical complexes combinations was realized, taking into account the capacity of the studied ligands to gain or lose one or several protons. Error tolerance was set at 1 mDa and identification of complexes was performed by confronting the experimental *m/z* on the average mass spectra to the "home-made" database.

2.3. Conductimetry experiments

Barium nitrate solution at 5 x 10^{-4} M and ligand solutions (DEGDE, VPA, or MAA) at 4 x 10^{-2} M were prepared in MeOH/water (1/1, v/v) or in ACN/DMSO (1/1, v/v). The complexation kinetics of four metal/ligand systems, each with a molar ratio M/L of 1/3, was studied: system A with $Ba(NO_3)_2$ and DEGDE in MeOH/water (1/1, v/v), system B with $Ba(NO_3)_2$ and DEGDE in ACN/DMSO (1/1, v/v), system C with $Ba(NO_3)_2$ and MAA in ACN/DMSO (1/1, v/v), and system D with $Ba(NO_3)_2$ and VPA in ACN/DMSO (1/1, v/v).
In order to obtain the system with the desired molar ratio, a known amount of ligand solution was added to 8 mL of salt solution under magnetic stirring (300 rpm). The evolution of conductivity versus time was recorded at regular intervals (5 min) for up to 48 h from the addition of the ligand solution. Measurements were performed in an air-conditioned room (21°C) with a SevenCompact S230 conductivity meter (Mettler Toledo, Viroflay, France) and a Pt electrode with a glass body (InLab® 720 having a measurement range from 0.1 to 500 µS cm^{-1}). The electrode was previously calibrated using a 10^{-3} M solution of KCl in Milli-Q water (148 µS cm^{-1} at 25°C).

2.4. ICP-MS analyses

Analyses were mainly performed using an Agilent 7700x ICP-MS (ICP-(CC)-Q-MS) equipped with a quartz concentric nebulizer and a quartz Scott spray chamber. A daily performance check (sensitivity, oxide and double-charged ion formation) was realized with an Agilent tuning solution. For the test on radium combined to the deeper evaluation of the specificity, measurements were realized on an Agilent 8800 ICP-MS/MS (ICP-QQQ-MS). In this case, ICP-MS was run in single quadrupole mode, using a desolvating system (Apex Omega) with a PFA MicroFlow nebulizer (Elemental Scientific (ESI)) operating in self-aspiration mode (~300 µL min^{-1}) as sample introduction system. To minimize the consumption of ^{226}Ra solution, the instrument was optimized with a uranium solution (1 µg L^{-1}) and then fine-tuned with a pure ^{226}Ra solution. Acquisition parameters of the two ICP-MS instruments are given in Table S1. From the analysis of 10 blank solutions (0.5 M HNO_3), the instrumental limits of quantification (LOQs) were calculated from Eq. (1). Values were estimated to be 0.03 µg L^{-1} for Ba in ICP-(CC)-Q-MS, and 17 mBq L^{-1} for ^{226}Ra in Apex Omega-ICP-QQQ-MS.

$$LOQ = \frac{\mu_{blank} + 10\sigma_{blank}}{a} \qquad \text{Eq. (1)}$$

where μ_{blank}, σ_{blank}, and a are the average number of counts per second (cps) in the analyzed blank solution, the corresponding standard deviation (cps), and the sensitivity of the instrument (cps/(µg L^{-1}) or cps/(mBq L^{-1})), respectively.

2.5. Solubility tests

Solubility tests for five polymerization mixtures (A–E) were performed using an initial volume of 0.75 mL of solvent for 0.125 mmol of barium nitrate salt, and varying the nature of solvent (ACN, 2-methoxyethanol, DMSO, MeOH, ACN/DMSO (1/1, v/v), ACN/MeOH (1/1, v/v), and MeOH/water (1/1, v/v)), and volume if necessary. Results of the ESI-MS complexation studies allowed to retain preferentially some ligand(s) and some template ion/monomer ratios, and DVB combined with styrene, and AIBN were chosen as crosslinking agent, co-monomer and polymerization initiator, respectively: $Ba(NO_3)_2$/MAA/styrene/DVB, molar ratio 1/10/20/20 (mixture A); $Ba(NO_3)_2$/DEGDE/styrene/DVB, 1/4/20/20 (mixture B); $Ba(NO_3)_2$/VPA/styrene/DVB, 1/6/20/20 (mixture C); $Ba(NO_3)_2$/DEGDE/MAA/styrene/DVB, 1/4/3/20/20 (mixture D); and $Ba(NO_3)_2$/DEGDE/VPA/styrene/DVB 1/4/3/20/20 (mixture E).

For each mixture, the solvent was added to the salt and the first ligand and the solution was then left under magnetic stirring for 24 h so that complexation may occur. Twenty-four hours later, if the salt was completely dissolved, the second ligand (MAA or VPA) was added to the mixture and the solution was left under magnetic stirring for another 24 h. If not, the volume of solvent and the complexation time were increased until a clear mixture was obtained before addition of the second ligand. If the mixture was still not clear after addition of a total volume of 2 mL of solvent, the test was abandoned and the mixture was considered not soluble in the studied solvent. Such a volume was indeed considered too high for IIPs synthesized by free radical bulk polymerization from 0.125 mmol of template ion. Styrene, DVB and AIBN (1% based on total moles of polymerizable double bonds) were finally added to the mixture. The tube containing the mixture was placed in a thermostatically controlled water bath at 60°C for 24 h to check whether polymerization was taking place and whether the resulting block polymers were homogeneous.

2.6. Synthesis of the ion imprinted polymers

Five IIPs were synthesized in ACN/DMSO (1/1, v/v) using Ba^{2+} as template ion and variable template/monomer(s)/co-monomer/cross-linker molar ratios (T/M/CM/CL) depending on the monomer(s) nature (Table 1). Another polymer, perfectly similar to IIP V, was synthesized using Ni^{2+} as template ion in place of Ba^{2+}, named IIP Ni, and used as another kind of control polymer. $Ba(NO_3)_2$ or $Ni(NO_3)_2 \cdot 6H_2O$ (0.5 mmol) and 3 mL of an ACN/DMSO (1/1, v/v) mixture were used as template and porogen, respectively. DEGDE, MAA, VPA and styrene, or a combination of them were used as monomers, DVB as cross-linker, and AIBN as initiator. The template was dissolved in the porogen and the first monomer was immediately added. The mixture was left under magnetic stirring for 48 h (24 h for solubilization followed by 24 h for complexation) before adding the second monomer (magnetic stirring for another 24 h). Afterwards, the cross-linker and the initiator (1% based on total moles of polymerizable double bonds) were added and the polymerization mixture was purged with nitrogen for 10 min to eliminate dissolved oxygen. The tube was finally sealed and immersed in a thermostatically controlled water bath at 60°C for 24 h to perform thermal polymerization. All NIPs were synthesized following the same protocol but without introducing template ions.

Table 1: Compositions of the six IIPs synthesized in ACN/DMSO (1/1, v/v) as porogen. The corresponding NIPs D, M, V, DM and DV were synthesized in the same conditions without introducing the template.

IIP name	Template ion (T)	Monomer(s) (M)	Co-monomer (CM)/Cross-linker (CL)	Ratio T/M/CM/CL
D	Ba(II)	DEGDE	Styrene/DVB	1/4/20/20
M	Ba(II)	MAA	Styrene/DVB	1/10/20/20
V	Ba(II)	VPA	Styrene/DVB	1/6/20/20
DM	Ba(II)	DEGDE/MAA	Styrene/DVB	1/4/3/20/20
DV	Ba(II)	DEGDE/VPA	Styrene/DVB	1/4/3/20/20
Ni	Ni(II)	VPA	Styrene/DVB	1/6/20/20

Once the polymers (IIPs and NIPs) were synthesized, they were crushed and automatically ground with a grinder MM 301 (Retsch®, Eragny sur Oise, France) at 30 Hz, and stirred for 3 cycles of 20 h in 3 M HNO_3 in order to remove the template ions from the IIPs. After each cycle, both IIPs and NIPs elimination solutions were filtered under vacuum with a Millipore glass filtration system surmounted by a MF-Millipore® mixed cellulose esters membrane filter (47 mm diameter, 1.2 µm pore size, Merck), and diluted 10^6 times with 0.5 M HNO_3 for subsequent ICP-MS analysis to assess the amount of barium template removed. Particles were then washed with UP water until the pH was neutral (estimation with pH paper), and dried in an oven at 50 °C. Next, polymers were sieved in a vibratory sieve shaker AS 200 from Retsch® (amplitude of 13 mm g^{-1}). Particles with sizes between 25 and 36 µm were finally sedimented in 20 mL of a MeOH/water mixture (80/20, v/v) (6 times for 90 min) to eliminate the smallest residual particles, before being dried again in an oven at 50 °C. Once dried, 30 mg of each polymer were packed in a 1 mL polypropylene cartridge (Merck) between 2 polyethylene frits (20 µm porosity, Merck) using 1 mL of MeOH, ready to be characterized by SPE.

2.7. SPE procedures in pure media

The five synthesized IIPs/NIPs were first evaluated by applying the same SPE procedures, in particular by comparing their retention properties in different percolation media: a mixture of ACN/DMSO (1/1, v/v) corresponding to the porogen used during synthesis, 0.56 mM of NH_3 at pH 10 or 25 mM of Bis-Tris buffer at pH 7. In optimal conditions for the most promising IIP/NIP, cartridges were conditioned with 3 mL of 25 mM Bis-Tris buffer at pH 7. 1 mL of the same buffer containing at most some tens of ng of each element was then percolated. Washing steps consisted in 0.5 mL of UP water, followed by 0.5 mL of HNO_3 at pH 4. The elution steps were finally carried out with 0.5 mL of HNO_3 at pH 3, 0.5 mL of HNO_3 at pH 2, and 1.5 mL of 0.5 M HNO_3. A flow rate around 0.5 mL min^{-1} was applied all along the procedure. After each use, cartridges were washed with water until pH was neutral and stored in UP water. Each collected fraction was diluted with 0.5 M HNO_3 before ICP-MS analysis in order to have a final element concentration staying within the calibration values. The recovery rate in each SPE fraction was calculated by comparing the amount of a given element in the fraction to the amount of the same element in the percolation solution using the calibration curve. For the test on radium, a multi-elemental solution containing ^{226}Ra at 0.01 Bq mL^{-1} and 36 elements at 10 µg L^{-1} in 25 mM of Bis-Tris buffer at pH 7 was loaded and extraction recoveries were determined from the counts per second measured in each fraction.

2.8. Physical characterizations

Thermogravimetric analyses (TGA) were realized under nitrogen atmosphere on a TGA 2 STAR^e system (Mettler Toledo, Viroflay, France) to evaluate the degradation temperature of the polymers. The loss of mass in function of the temperature was recorded using up to 5 mg of initial sample mass and applying a heating ramp of 5 °C min^{-1} until a maximum temperature of 600 or 800 °C was reached.

The Brunauer-Emmett-Teller (BET) nitrogen adsorption/desorption technique was also applied on some of the prepared polymers to evaluate their BET surface area (S_{BET}) using a 3-Flex system (Micromeritics®, Merignac, France). 100 mg of sample were weighted in a sample holder and placed on a port of the instrument for *in situ* degassing under vacuum by applying the following heating program: 25-60 °C at 10 °C min^{-1}; 60-150 °C at 5 °C min^{-1}; 150-180 °C at 2 °C min^{-1}; and 180°C for 1 h. S_{BET} values were calculated for P/P° values in the range 0.05–0.35, the range in which the curve obtained is linear and the BET model is valid. The samples were reweighted at the end of the analysis to calculate the S_{BET} values from dry sample masses.

3. Results and discussion

3.1. Screening of the synthesis conditions

3.1.1. Choice of the best monomer candidates by MS experiments

As previously mentioned, Ba^{2+} was selected as a Ra^{2+} analogue for the development of the IIPs, mainly for radiological protection reasons and since its size and chemical properties makes it the best analogue candidate. The binding affinity of different monomer-ligands for Ba^{2+} was tested by direct infusion ESI-MS in order to select the best candidates for further IIP syntheses. This technique has the advantage to be currently present in almost all laboratories and allows to produce rapid results as analyses are fast and data treatment may be automated. Those four limits or constraints must however be considered: (i) the solvent of the studied medium must be compatible with the ionization source, (ii) detected complex lie in the gas phase and may be different in solution, (iii) neutral or too weak complexes are not visible, and (iv) analyses remain qualitative as no commercial standards exist. Four commercial ligands (DEGDE, MAA, 2-VP and VPA), some not being conventional in IIP synthesis, and exhibiting various structures and acido-basic properties were selected. DEGDE is an acyclic ether with three oxygen atoms as possible interaction sites and was selected to test whether it can form ML_n complexes (n≥2) with Ba^{2+}. It was picked in order to recreate a pseudo-crown ether upon complexation since crown ethers are known to efficiently trap alkaline earth metals (e.g. 21C7 for Ba^{2+} and Ra^{2+}) [38,42]. However, crown ethers bearing a vinyl function are not commercially available, thus preventing their use as monomers. MAA possesses a carboxylate group (pKa: 4.66) and is the most common monomer used both for molecularly imprinted polymer (MIP) and IIP synthesis. 2-VP can develop interactions with cations *via* its π-bonds and the free doublet of its nitrogen atom (pKa: 4.86) while VPA has several electron donor moieties involving oxygen atoms on its phosphorus group (two hydroxyl groups with pKa values of 3.68 and 8.70, and a P=O double bond). Polydentate amino carboxylic acids and phosphorus-based extractants are indeed known to complex well Ra^{2+} involving electrostatic forces and the right coordination number [38]. Among the studied systems, some were only with one kind of ligand and other with two kinds of ligands (DEGDE combined to MAA, 2-VP, or VPA), the role of the second ligand being to enhance the specificity of the complex. Apart from the ligand(s) nature, the influence of two other parameters on complex formation was also studied, namely the metal/ligand molar ratio and the complexation time before infusion. It should be noted that these experiments were carried out in MeOH/water (1/1, v/v) rather than in potential synthesis solvents for reasons of compatibility with the ESI source. Thus, the obtained results were carefully interpreted keeping in mind that solutions were not strictly representative of the polymerization medium due in particular to the solvent nature and to the low concentrations of template and monomer(s). MeOH and water are indeed generally not used for IIP synthesis because their polar and dissociative character may affect template-monomer interactions. However, as shown in Table 2, several complexes were detected in this medium. Detailed results of species identified for each system as a function of the ligand ratio and the incubation time are provided in supplementary information (Table S2 to S8).

All solutions were infused in the softest ionization conditions with the aim of keeping complexes intact. Extracted ion chromatograms (EICs) performed on scan of *m/z* 60–900 resulting from the data processing exhibited either a continuous signal over the entire infusion period, a discontinuous signal, or no signal. As the background noise of the instrument was in the order of 10^5, only signals with higher intensity than this threshold value allowed to confirm the presence of complexes. A discontinuous signal could indicate that the corresponding complex was not stable or not easily ionizable, therefore we did not take into account such complexes when selecting the monomers for future syntheses. These results, summarized in Table 2, indicate that a great variety of complexes were observed, notably with DEGDE (2 species), MAA (5 species) and VPA (6 species) alone, but also mixed complexes for Ba^{2+}/DEGDE/MAA (8 species) and Ba^{2+}/DEGDE/VPA systems (4 species). As no standard exists, it was not possible neither to quantify the proportion of each complex nor their stability constant with this technique. Assuming the bonds occur *via* O-atoms, some of the previously cited complexes have a stoichiometry in close agreement with the coordination number of Ba^{2+} (8), such as $[Ba+2DEGDE+2MAA-H]^+$ or $[Ba+2DEGDE+VPA-H]^+$ [21]. Almost no complex containing 2-VP was observed. This could mean (i) that the only ligand containing a nitrogen atom has less affinity for Ba^{2+} than the three other oxygen atom ligands studied, or (ii) that only neutral complexes were formed and could therefore not be detected with that technique, or else (iii) that complexes formed were either difficult to ionize, or (iv) not stable and destroyed in the ionization source. Since we had no more information, we decided not to pursue next steps of the screening synthesis conditions with this ligand but we kept all the other ones.

Table 2: Barium complexes identified in ESI(+/-)-MS depending on the ligand(s) (L). Data treatment was realized on one infusion for each ligand(s) system.

Ligand(s) (molar ratio)	**Identified complexes**
DEGDE	$[Ba+nL]^{2+}$, n ∈ {2, 3}
MAA	$[Ba+nL-H]^{+}$, n ∈ {1, 2, 3, 4} $[Ba+3L-3H]^{-}$
2-VP	$^{a}[Ba+3L]^{2+}$
VPA	$[Ba+nL-H]^{+}$, n ∈ {1, 2, 3, ^{b}4, ^{b*}5, ^{a*}6}
DEGDE/MAA (4/3)	$[Ba+nL1+L2-H]^{+}$, n ∈ {1, 2} $^{c*}[Ba+nL1+L2]^{2+}$, n ∈ {1, 2, 3} $^{c*}[Ba+2L1+2L2]^{2+}$ $^{c*}[Ba+L1+3L2-H]^{+}$ $^{*}[Ba+2L1+2L2-H]^{+}$
DEGDE/2-VP (4/3)	$^{c*}[Ba+L1+2L2]^{2+}$
DEGDE/VPA (4/3)	$^{c}[Ba+L1+L2-H]^{+}$ $^{c*}[Ba+L1+2L2-H]^{+}$ $[Ba+2L1+L2-H]^{+}$ $^{c*}[Ba+2L1+L2]^{2+}$

*: Signal not continuous over the entire infusion period.
^{a}: Specie only detected in the solution with a molar ratio of 1/6 and infused after a long complexation time.
^{b}: Specie only detected in solutions with a molar ratio of 1/6, whatever the complexation time.
^{c}: Specie only detected for the solution infused after a short complexation time.

The maximum stoichiometry observed for Ba^{2+}/DEGDE, Ba^{2+}/MAA and Ba^{2+}/VPA complexes were 1/3, 1/4, and 1/6, respectively. The steric hindrance and the fact that solvent in which solutions were prepared was not pure water may explain why the 8-fold Ba^{2+} coordination number was not reached. Another explanation could be that bigger complexes tend to be less stable in the source and thus more difficult to see. Indeed, we noticed that the signal intensity decreases and becomes discontinuous when the complex contains a greater number of ligands molecules (e.g. from 5 VPA molecules or more bound to Ba^{2+} in Figure S1). Though many complexes were visible, it is evident that only one or two species predominate both in solution and in the source. Considering for instance the system Ba^{2+}/VPA, ML_6 or bigger complexes which are close to the 8-fold coordination number of Ba^{2+} may break in the source that is why ML_1 to ML_5 complexes are also visible.

Only complexes bearing a single charge (one ligand lost one proton) or doubly charged (only composed of neutral ligands) were monitored. If we assume that the pH in MeOH/water is closed to 5.5-6 (pH of UP water) and considering pKa values previously mentioned, DEGDE is neutral in solution, MAA exists in both its neutral and anionic deprotonated forms, 2-VP exists in both its neutral and cationic protonated forms, and VPA mostly exists in both its anionic form (loss of only one proton) and its neutral form. This is consistent with complexes reported in Table 2. Indeed, complexes containing a majority of neutral ligand molecules were mainly observed in the positive ionization mode and this can be explained by in source reprotonation (e.g. H^+ coming from the solvent). An example of average mass spectrum on which the state of charge of a Ba^{2+} and DEGDE-based complex is visible, is provided in Figure S2.

As expected, solutions with the greatest M/L molar ratio led to the formation of the biggest complexes (e.g. species marked a and b in Table 2). Regarding systems involving a single ligand, the complexation time seemed not have any significant effect on the formation of complexes since the same species were generally identified on the mass spectra of solutions infused after 2 h and after 24 h of incubation (see Tables S2 to S5 in supplementary information). Therefore, the kinetics of complexation seem to be fast in MeOH/water (1/1, v/v). In case of systems combining two different ligands, the influence of the incubation time was less clear (see Tables S6 to S8 in supplementary information). We noticed for instance that some species were only detected after a short incubation time (e.g. species marked c in Table 2), perhaps because they were then supplanted by other more stable complexes.

To conclude, this study based on MS measurements allowed to eliminate 2-VP and to keep as monomer-ligands VPA, MAA, and DEDGE alone or a combination between DEGDE and VPA or MAA, which correspond to 5 different conditions of IIP synthesis. The selection of these functional monomers was made in agreement with the stoichiometry of the observed species and the Ba^{2+} coordination number.

3.1.2. Choice of the synthesis solvent

Once some monomers were selected, the best candidates being VPA, MAA, and DEDGE alone and VPA or MAA combined with DEGDE for previously mentioned reasons, solubility tests of the different polymerization mixtures were conducted to determine in which solvents (nature and volume) syntheses should be performed. For solvent selection, we used a 2D-map representing the dielectric constant in function of the polarity index of typical solvents used for MIP and IIP synthesis (Figure S3). To have more chance to dissolve the barium nitrate salt in organic solvents, 6 porogens all rather quite polar but covering a wide range of dissociating power were selected either alone (ACN, 2-methoxyethanol, and MeOH), or in mixture (ACN/MeOH, ACN/DMSO, and MeOH/water, all with a ratio 1/1, v/v). Even though MeOH/water is known to be a polar and protic solvent, which also tends to dissociate compounds, according to the MS results we were able to observe complexes in this medium. It was thus included in the porogen candidates list. Indeed, if it could solubilize compounds and lead to the formation of cavities, then reproducing later the ionic recognition mechanism when putting the IIPs in contact with an aqueous sample would be easier that in case of IIPs synthesized with organic solvents.

For most of the solubility tests, monomers were introduced slightly in excess compared to the stoichiometry of complexes observed in MS, in order to favor the formation of species respecting the coordination number of Ba^{2+} while not risking that too many ligands remain uncomplexed.

DVB was selected as cross-linker instead of ethylene glycol dimethacrylate (EGDMA) which possesses several O-atoms and could thus be a source of non-specific interactions. It was also demonstrated in a paper dedicated to the reusability of MIPs that polymers synthesized with DVB were more resistant under acidic and basic extraction conditions than those with EGDMA which are subjected to hydrolysis [43]. In literature, DVB is usually employed in combination with styrene monomers [44–47]. Therefore, a styrene/DVB molar ratio of 1/1 was applied as it allowed to form a polymer structure with well-defined cavities as already demonstrated for instance for a samarium IIP [45] and an uranyl IIP [46] compared to an excess or deficit of DVB. Various template/DVB/styrene molar proportions were employed (e.g. 1/20/20 [45], 1/30/30 [44], 1/40/40 [46], and 1/65/65 [47]) but, as there is a lack of hindsight on the effect of this ratio in the reported works, we decided to keep the one corresponding to the most used T/CL ratio (1/20). However, among the 6 porogens tested, only 0.75 mL of ACN/DMSO (1/1, v/v) (polar and aprotic) allowed to solubilize the 5 polymerization mixtures depicted in section 2.5 and containing 0.125 mmol of barium. This volume of 6 ml per mmol of template is consistent with other IIPs synthesized by bulk polymerization from 1 mmol of template : 3.6 mL for a zinc IIP [48], 4.3 mL for a calcium IIP [33], 5 mL for lanthanide IIPs [45,49], 5.6 mL for a potassium IIP [50], 8.3 mL for a zinc IIP [51], and 10 mL for iron [44], lanthanides [35,52], and zinc IIPs [53–55]. Consequently, all barium IIPs were synthesized in this porogen.

3.1.3. Choice of the complexation time

Kinetic studies were then carried out by conductimetry to confirm the formation of complexes in the selected porogen and also to determine the complexation time between Ba^{2+} and the monomer(s) in this medium. This technique is easy to implement and is efficient as soon as the sensor used is able to detect a change in conductivity. The Figure 1 shows the conductivity trend depending on the studied system. A moving average was considered to filter the noise of the acquired data. The complexation time, indicated on the figures, was defined as the moment when the conductivity begins to stabilize and that materializes by a slope discontinuity. Experiments in ACN/DMSO (1/1, v/v) demonstrated that DEGDE-based complexes take around 16 h to form (Figure 1a), while those with MAA (Figure 1b) and VPA (Figure 1c) require only 80 and 40 min, respectively. The changes in conductivity after addition of the ligand were sometimes low but as the conductivities measured in both pure salt and ligand solutions were constant and the precision of the electrode was 0.1 µS cm^{-1}, observed changes were considered significant. Depending on the monomer, an increase or decrease in conductivity was observed until a plateau was reached. The molar ionic conductivity being proportional to the mobility of the ion (Nernst-Einstein equation), these evolutions can be interpreted based on the ionic mobility of the free ions and complexes, previously observed in MS, present in the solution knowing the following equation (Eq. (2)).

$$\mu = \frac{|q|}{k\eta} \qquad \text{Eq. (2)}$$

where µ, $|q|$, k and η are the mobility of the complexed ion (m^2 s^{-1} V^{-1}), the absolute value of the metal ion charge (C), a positive parameter proportional to the radius of the solvated complex (m), and the viscosity of the medium (Pa s), respectively.

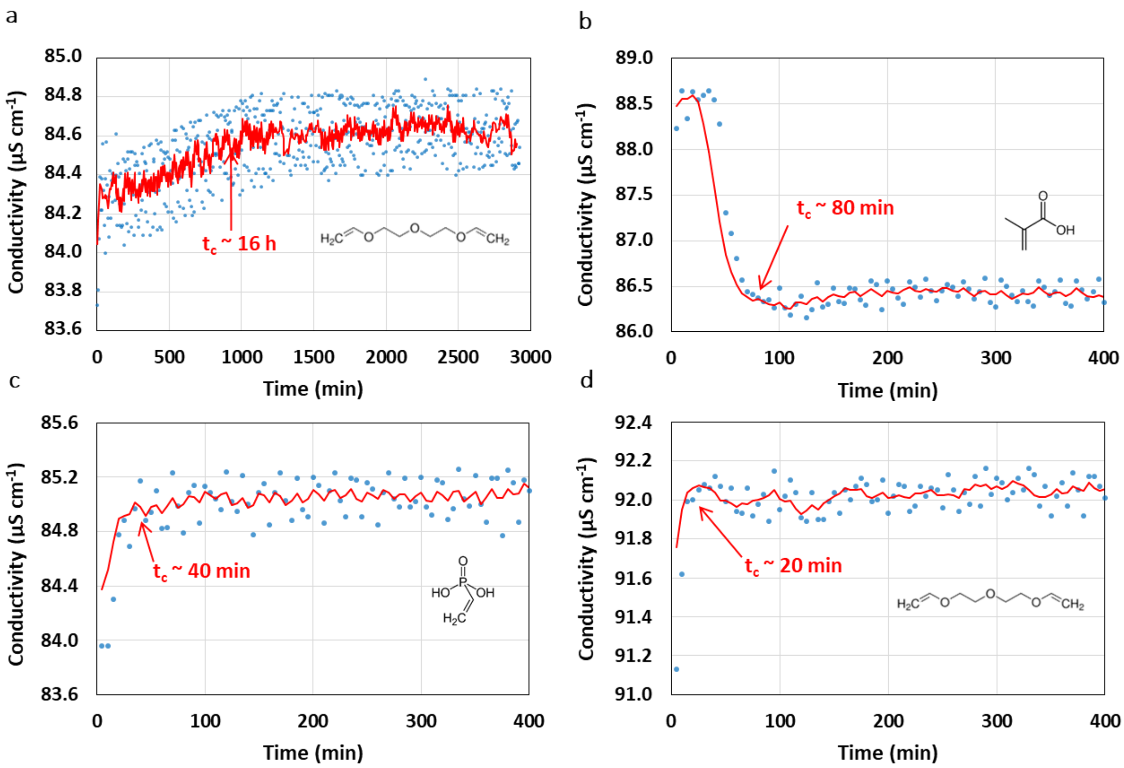

Figure 1: Complexation kinetics of Ba^{2+} by the ligand DEGDE (a), MAA (b), and VPA (c) in ACN/DMSO (1/1, v/v), and by DEGDE in MeOH/water (1/1, v/v) (d). t$_c$: complexation time. The red curve represents a 5 points moving average. At a given time T_i, the moving average was calculated considering the N following conductivity values at times $T_i, T_{i+1} = T_i + 5\,min, \dots T_{i+N-1} = T_i + (N\text{-}1) \times 5\,min$. Each plot corresponds to one kinetic experiment.

For each system, we deducted from the MS experiments the minimum and maximum number of ligands that could bind to Ba^{2+}. We also made an assumption on the charge of the ligands since in an organic medium the pH is not easy to measure. All interpretations were made considering that in the studied solutions DEGDE was neutral (compound having no ionizable function) and that MAA and VPA had both a negative charge. Considering for instance the Ba^{2+}/DEGDE system, the complexes are in the form $[Ba+xDEGDE]^{2+}$ with $x \in \{2,3\}$: the charge is unchanged while the size of the complex is larger than the one of the free ion. In theory, the mobility of the complexes should therefore be lower than that of the free ion and we should observe a decrease in conductivity in Figure 1a. On the contrary, a very slight increase was recorded, probably a sign that the parameter k must actually decrease due to solvation effects compared to the free ion. Following the same logic, the mobility of $[Ba+xMAA]^{2-x}$ complexes with $x \in$ {1-4} should decrease since the absolute value of the charge decreases (unchanged for x=4) and the size increases for all x. This was observed in Figure 1b. For $[Ba+xVPA]^{2-x}$ complexes with $x \in$ {1-6}, we should have an increase in charge and size for $x \in \{5,6\}$. Since the charge effect always dominates over the size effect, one should have an increase in mobility as observed in Figure 1c.

Figure 1 also shows the influence of the solvent on kinetics. Complex formation was indeed faster in MeOH/water (1/1, v/v) since the conductivity stabilized after only 20 min (Figure 1d) while the plateau was reached after 16 h in ACN/DMSO (1/1, v/v) (Figure 1a). These observations confirmed those made during the MS experiments performed in MeOH/water. Indeed, no significant differences were observed between the complexes detected during the infusion of solutions incubated for 2 h or for 24 h, both durations being higher than 20 min. Contrary to what was expected, it seems that the strong dissociating power of the MeOH/water mixture (1/1, v/v) promotes the dissociation of the $Ba(NO_3)_2$ salt and thus the access of the ligands to Ba^{2+} ions. Having less affinity for organic solutions than for aqueous ones, the salt may dissociate less rapidly in ACN/DMSO (1/1, v/v).

Since the measured complexation times were all between 40 min and 16 h in ACN/DMSO (1/1, v/v) and also in order to be in the same conditions for all syntheses, it was decided to keep a complexation time of 24 h after each addition of monomer, independently of its nature.

3.2. Performance comparison of the synthesized IIPs

After the selection of the monomers-ligands, the nature and volume of the porogen, and the complexation time, five IIPs and their corresponding NIP were synthesized using Ba(II) as template ion and conditions described in Table 1. Polymers were ground before proceeding to three cycles of 20 h of washing with 3 M HNO_3 to remove the template ions. The amount of ions determined by ICP-

MS in the IIP and NIP elimination solutions are available in Table S9. More than 80% of template ions introduced during the synthesis were removed after the first two elimination cycles and the third cycle was often ineffective to release the rest of ions bound to IIP cavities (e.g. IIPs V, D, and M). Removal efficiencies greater than 100% can be explained by the fact that during filtration of the first elimination solution, polymer particles remain impregnated by the solution of the first elimination cycle, thus distorting the quantification during the measurement of the elimination solution corresponding to the second and third cycles. Ba(II) ions were not measured in the elimination solutions recovered from the NIPs, evidencing that there was no contamination during their synthesis.

After sieving and sedimentation steps, 25-36 µm particles were packed in cartridges (30 mg of sorbent) for their characterization that consists in studying the retention of Ba^{2+} on each sorbent by analyzing the percolation, the washing and the elution fractions of a SPE procedure. A SPE procedure was first performed on a non-spiked sample (blank) to ensure cartridges were clean before starting the characterization of the polymers. SPE profiles obtained using IIP M are not reported because of the lack of repeatability of the results. Indeed, during the synthesis, the barium nitrate salt did not solubilize completely contrary to what happened during the solubility test of the corresponding polymerization mixture. The synthesis of this IIP has therefore been redone but the salt solubilization was still not complete. These solubilization problems had an effect on the obtained SPE profiles as they were not similar which can be explained by the fact that incomplete solubilization of the template ions must have led to different IIP structures. Therefore, this IIP was removed from this study.

The optimization of the SPE protocol was done in order to evaluate and compare the performances of the four other supports in terms of retention, selectivity (*i.e.* difference of retention between IIP and NIP), and specificity (*i.e.* difference between targeted and interfering ions). Regarding the last point, to limit extensive data processing and security constraints, the polymers were first evaluated by comparing the extraction profiles of only two model ions: Ba(II) which was used as template and is also a good analogous of the target ion (Ra(II)), and Cs(I) as interfering ion, the closest alkali metal to Ra(II) in the periodic table. The first step of the optimization of the SPE procedure consisted in finding an ideal percolation medium favoring the retention of at least Ba(II). Since ACN/DMSO (1/1, v/v) was used as porogen for all syntheses, this medium was first used for percolation in order to recreate the target ion-monomer interactions that allowed the formation of the hypothetical cavities during the syntheses, as it is usually done in the case of MIPs. In order to gradually disrupt these interactions, several washing and elution steps with 0.5 mL of HNO_3 at decreasing pH, from pH 4 to pH 2, and with 3 mL of 0.5 M HNO_3 were applied. However, none of the ions could be retained in this percolation medium on any of the four IIPs and their NIP (Figure 2 a1, b1, c1, and d1). For the IIPs D (Figure 2a1) and DV (Figure 2c1), the Ba(II) recovery yield was much higher than 100%, indicating the presence of residual template ions which continued to be randomly released even after performing template ion elimination and SPE blanks. This phenomenon became negligible after several uses of the cartridge (usually 2 or 3 uses) and this did not prevent us from confirming the low retention of ions under these conditions on these two IIPs.

Among monomers employed, MAA (pKa: 4.66) and VPA (pKa: 3.68 and 8.70) bear acid moieties and can therefore establish electrostatic interactions with cations depending on the pH. In order to deprotonate the acid groups present in cavities, a new extraction procedure was carried out in a basic medium, by loading ions in an NH_3 solution at pH 10. In these conditions, Ba(II) was well retained on IIPs V (Figure 2b2), DV (Figure 2c2), and DM (Figure 2d2), up to the final elution step (E3), to elution step at pH 3 (E1), and to elution step at pH 2 (E2), respectively. Cs(I) was also less retained than Ba(II) on these three IIPs (almost unretained on IIPs DV and DM). This indicates a certain degree of specificity of the polymers, property that was further studied afterwards. It is interesting to note that only IIP V presented more retention for Ba(II) than its NIP, thus showing a difference in selectivity as expected, although the washing step had not yet been optimized. A difference between the SPE profiles of IIP DV and its NIP was also observed but not as expected as in this case, Ba(II) was more retained on the NIP than on the IIP. These results were confirmed by repeating twice this SPE procedure on IIPs/NIPs V and DV (the two consecutive bars in Figure 2b2 and c2 corresponding to results obtained in duplicate). At last, the retention on IIP D was still low for both ions in this percolation medium (Figure 2a2).

As at pH 10, many elements present in natural waters (targeted samples) could precipitate and risk in the same time to entail Ra(II), a 25 mM Bis-Tris buffer at pH 7 was also tested as alternative percolation medium in order to be closer to the pH of such samples. Bis-Tris was selected for its pKa (6.5 at 25°C) and because it is a cationic buffer and should thus not interact with cations. First, since these conditions also failed to retain Ba(II) on IIP D (Figure 2a3), it seems no cavity was formed even though DEGDE-based complexes were observed in MS. Characterization of this IIP was therefore not pursued. The SPE profile of IIP V showed Ba(II) was recovered in fractions E1 and E2 (Figure 2b3), so it was a bit less well retained than in NH_3 at pH 10, which can be explained by the fact that not all acidic groups of VPA-based cavities are negatively charged since pH is probably lower than pKa_2 of the polymerized monomer. However, a difference in selectivity with its NIP was still visible and Cs(I) mainly came out during the percolation (~60-70%) and washing steps, thus improving the specificity of the polymer and making the extraction procedure in Bis-Tris more interesting. Regarding the profiles of IIP DV (Figure 2c3) and DM (Figure 2d3), Cs(I) was still less retained than Ba(II), however the retention of Ba(II) decreased very strongly on these two supports to make this percolation medium attractive. Moreover, the selectivity of these IIPs in comparison with their NIP was not observed.

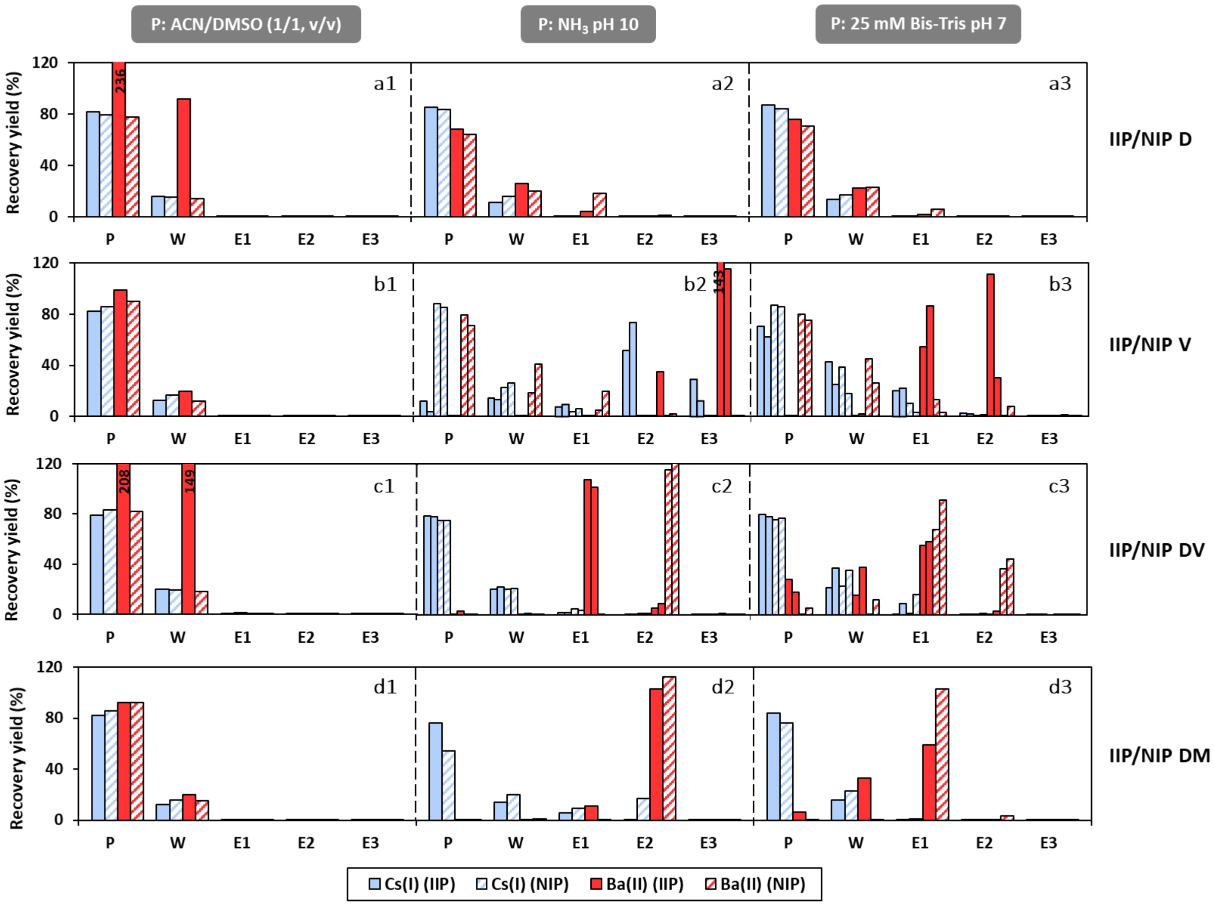

Figure 2: SPE profiles of Cs(I) and Ba(II) obtained on IIPs and NIPs D, V, DV, and DM by varying the percolation medium (a1, b1, c1, and d1: ACN/DMSO (1/1, v/v); a2, b2, c2, and d2: NH_3 solution adjusted to pH 10; a3, b3, c3, and d3: 25 mM Bis-Tris buffer at pH 7). P: percolation of 1 mL of test medium spiked with 25 µg L^{-1} of Cs(I) and Ba(II). W: washing with 0.5 mL of UP water and 0.5 mL of HNO_3 pH 4. E1 to E3: Elution with 0.5 mL of HNO_3 pH 3, 0.5 mL of HNO_3 pH 2, and 3 mL of HNO_3 0.5 M, respectively. Two consecutive bars of the same color are plotted when the procedure was repeated twice. All fractions were analyzed with an ICP-(CC)-Q-MS system (Agilent 7700x). Tl (*m/z* 205 monitored) at 0.1 µg L^{-1} was used as internal standard to correct matrix effects in solutions containing ACN/DMSO.

Therefore, we tried to modify the washing protocol while loading ions at pH 10 again to obtain a difference in selectivity between the IIPs and their NIP. The influence of pH was first investigated, in particular, the washing step protocol was changed with a gradual decrease in pH from 3 to 2 since it was between these two values that Ba(II) was recovered from IIP DV and DM in SPE procedures presented in Figure 2 c2 and d2. Six successive washing steps with a very gradual decrease in pH by 0.2 units from pH 3 to pH 2 were applied, but as exemplified in Figure S4, under these conditions both NIPs retained Ba(II) as much or more than the IIPs. This may result from non-specific interactions caused by the presence of numerous monomer moieties at the surface of the resulting polymers, especially if the surface areas are significantly different between the IIP and its NIP as it was already reported in literature [56,57] and will be studied latter in this paper.

As the presence of DVB and styrene in large proportion confers to polymers a hydrophobic character, a second trial was realized by adding a small proportion of organic solvent in the washing solutions in order to improve the access of Ba(II) ions to the cavities and thus promote interactions between these ions and the functional groups present in the formed cavities. For this purpose, a gradient of EtOH was implemented with mixed HNO_3 pH 4/EtOH solutions in proportion 95/5 to 60/40 v/v, but this did not enhance the retention on the DV and DM IIPs over that on the NIPs either (Figure S5). Given the behavior of crown ethers towards alkaline earth ions and based on the obtained MS results, we expected from these IIPs synthesized with a mix of monomers in order to form mixed complexes to be both more specific and selective than others. This difference in retention could be again explained by a difference in specific surface area between the IIPs and their NIP and/or by the mobility of the DEGDE monomers in cavities. DEGDE being an acyclic ether, it can indeed be more subjected to conformational changes than a crown ether, resulting in the case of IIPs, in cavities whose "shape" is not fixed.

Further SPE characterizations were thus only conducted on the most promising IIP, namely IIP V. A third extraction procedure in Bis-Tris was made to confirm the observed trends on that sorbent. In Figure S6, the recovery calculated for the first extraction was quite high (165%) due to the release of residual template ions as already mentioned, but started to stabilize after the second extraction (117% and 116% in experiments n = 2 and 3, respectively). This highlights the interest of using an analogous ion as template instead of the target ion when the final purpose is to measure traces with high precision. Most of the IIPs in literature are however still directly synthesized from the target ion. The total average recovery yield of Ba(II) on the NIP was also sometimes higher than 100% (138%, 112%, and 104% for n = 1, 2, and 3) and can be explained by contaminations coming from the equipments and solutions employed during post-synthesis steps (common crushing bowls, filtration system, and sieves as those used for the IIP treatment) or by the equipments used to prepare solutions and characterize sorbents (tubes, pipette tip cones, cartridges, etc.). These contamination issues are also valid for the IIP. Since Ba(II) is present everywhere in nature, adding a pre-washing step of the material with a nitric acid solution and a contact time of 24 h could actually solve this contamination issues. However, as it is time-consuming, we did not proceed like this during the development phase as the main goal was to identify the most promising imprinted polymer among all those synthesized.

In order to correlate the observed behavior in extraction of some IIPs and their NIP to their structure, TGA (Figure S7) and BET analyses (Figure S8) were conducted. TGA allowed to evaluate until which temperature it was possible to heat samples during the degassing phase that precedes a BET analysis. IIP and NIP V as well as IIP DV decomposed all from 300°C, meaning that the degradation temperature is only dictated by the main matrix components, the co-monomer and the cross-linker. BET experiments demonstrated that polymers display very different surface areas in the order of 7 to 352 $m^2\ g^{-1}$ (Table 3). Although uncertainty on the specific surface area of IIP V is high (see more details in supporting information), main information is that surface area of NIP V is about 15 times greater, indicating they have different structures. Therefore, the synthesized NIP does not completely correspond to an ideal control polymer.

Table 3: BET surface areas determined by nitrogen adsorption/desorption experiments of some polymers. Uncertainties estimated from specifications provided by the constructor and summarized in Table S10. For each polymer, only one measurement cycle was performed.

Polymer	S_{BET} ($m^2\ g^{-1}$)	Absolute S_{BET} in the sample holder (m^2)
IIP V	7 ± 5[a]	0.6 ± 0.5[a]
NIP V	102 ± 4[b]	9 ± 0.3[b]
IIP Ni	3 ± 2[a]	0.3 ± 0.2[a]
IIP DM	80 ± 6[c]	7 ± 0.5[c]
NIP DM	352 ± 13[b]	33 ± 0.3[b]

[a]: An uncertainty of 76% was considered as the absolute surface value was close to 0.5 m^2.
[b]: An uncertainty of 3.8% was considered as the absolute surface value was close to 10 m^2.
[c]: An uncertainty of 7.6% was considered as the absolute surface value was close to 5 m^2

The synthesis of a more suitable control polymer using nickel as template ion (named IIP Ni) but keeping all the other synthesis conditions equal to IIP V was investigated. SPE profile in Figure S9 (same extraction conditions as these of SPE procedure in Figure 2b3 on IIP V and NIP V) demonstrated a pretty good imprinting effect as the totality of Ni(II) was retained against only 40% for Ba(II). Taking into account the uncertainty of the measurements, it can be mentioned that the surface area of IIP Ni (3 $m^2\ g^{-1}$, see Figure S8d and Table 3) was of the same order of magnitude as that of IIP V, indicating it could be employed as an alternative control polymer.

BET results also confirmed that NIP DM has a much greater surface area than its IIP (352 against 80 m^2), which can explain why it retains more strongly Ba(II) as mentioned earlier. Apart from IIP V, S_{BET} of the developed polymers are in the bottom bracket compared with other IIPs/NIPs in literature, which have most of the time surface areas of several tens to several hundreds of $m^2\ g^{-1}$ [28,30,58]. IIPs having surface areas of a few $m^2\ g^{-1}$ have however already been reported in literature [40,57,59,60]. Making comparisons remains difficult since many factors can influence the surface area of an IIP, including the reagents used for the synthesis and their proportion, the synthesis approach (e.g. bulk *versus* IIP coating at the surface on another material), the treatment undergone after synthesis, and the degassing method employed. This last element is for instance not always specified in publications.

3.3. Further characterization on the most promising polymer: IIP V

3.3.1. Study of the specificity in presence of radium and a large range of competitors

Competitors with different charges, sizes, properties, or possibly source of spectral interferences in ICP-MS, were selected to further investigate the selectivity and specificity of IIP V and its NIP. A multi-elemental solution containing ^{226}Ra(II), but also Ba(II) and 16 competing ions from almost all families of the periodic table (Li(I), Rb(II), Cs(I), Sr(II), La(III), V(V), Co(II), Nb(V), Mo(VI), Ag(I), W(VI), As(V), Sb(V), Tl(I), Pb(II), and Bi(III)) was loaded on IIP/NIP SPE cartridges. Analyses were this time performed with a desolvating nebulizer rather than with a traditional Scott spray chamber in order to enhance signal sensitivity for ^{226}Ra measurement and further eliminating potential spectral interferences. The selectivity of the IIP V was confirmed for Ra(II) ions as they were retained by the IIP but not by the NIP (73% against 5% in fraction E1+E2), which demonstrate the presence of cavities in the IIP V formed using Ba(II) as template and able to trap Ra(II) ions (Figure 3a). Except La(III), ions were not retained on the control polymer (NIP), proof of the absence of non-specific interactions.
Regarding now the IIP, it can be observed that alkali metals (Figure 3a), most of the transition metals (Figure 3b: V(V), Nb(V), Mo(VI), and W(VI)), and metalloids (Figure 3c: As(V) and Sb(V)) tested were not retained on the sorbent. Alkali metals should have less affinity for the sorbent due to their single charge. Being able to discriminate them is attractive since they are among the most abundant elements in nature. Removing Mo(VI) and W(VI) is also of great interest as they may form the following argides at *m/z* 226 in the plasma: $^{92}Mo^{94}Mo^{40}Ar^{+}$ and $^{186}W^{40}Ar^{+}$. However, the specificity remains partial because some other elements, such as La(III), Co(II), Ag(I), Tl(I), and Pb(II), were co-extracted, Bi(III) being also more retained than Ba(II) and Ra(II). It is worth noticing that in the case of La(III), non-specific interactions may occur as it was also retained by the NIP. For the other ions, as they were retained on the IIP V and not on the NIP, they may enter into the specific cavities. As several parameters are involved in the retention process, namely the charge, the hydrated ion size,

the coordination number, the effect of solvent, the nature of atoms (hard or soft), and orbitals, the interpretation of observed behaviors remains difficult. The specificity of the VPA-based IIP may be explained by the number of ligands present in the cavity that is close to the coordination number of Ra^{2+} (6 against 8), in combination with the charge and size of the cavity and the affinity of Ra^{2+} for the O-atoms of the P-O and P=O bonds that are highly polarized.

As a remark, Sr(II), Tl(I), and Pb(II) also have affinity for the commercial AnaLig® Ra-01 resin, which is currently the most specific SPE support available for Ra(II) extraction. However, Verlinde *et al.* were able to find successful conditions to eluate these interfering ions before Ra(II) [16]. Some attempts were thus made to modify the washing conditions in order to improve the specificity as it will be described in section 3.3.2. Polymers affinity for U and Th actinides elements were also investigated but results are not presented here as they were both retained on the imprinted and control polymers but with uncomplete total recoveries (maximum 40% and 20% recovered respectively). These elements are known to be complicated since they are not stable at neutral and basic pH (e.g. they can form precipitate and adsorb onto walls of tubes and cartridges depending both on the constituent material and the given conditions) and thus we did not take into account information about them in these extraction conditions.

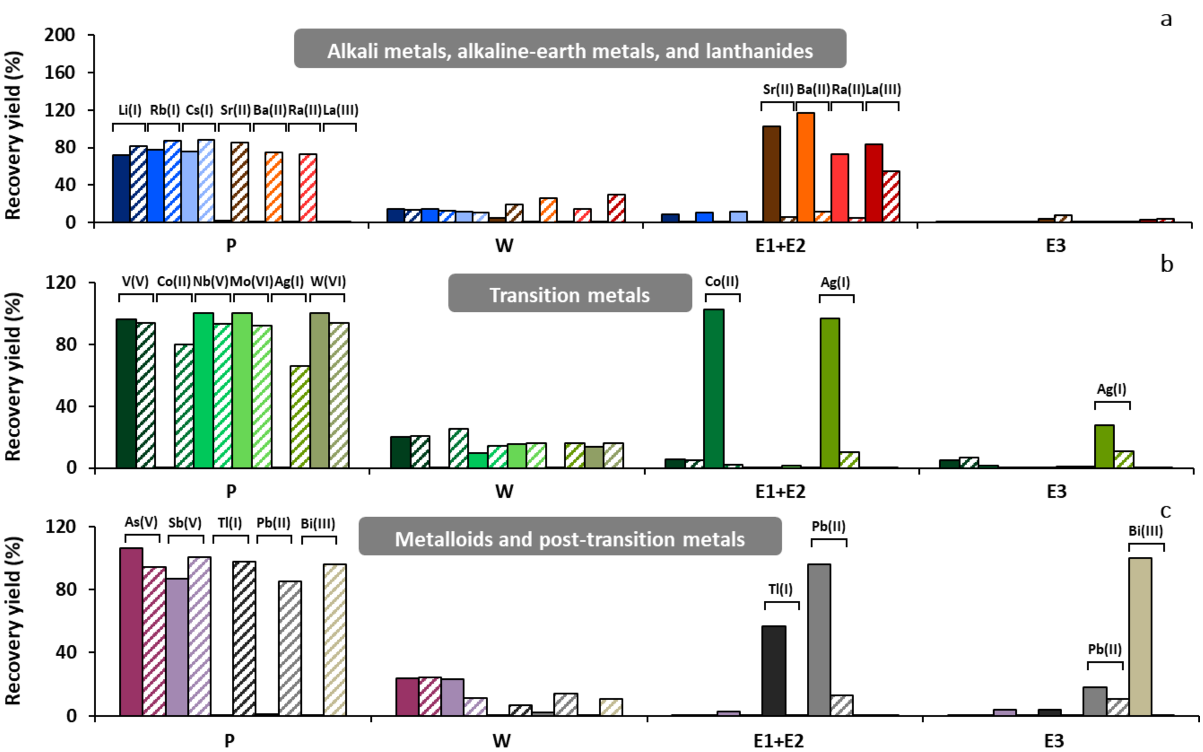

Figure 3: SPE profiles of various alkali metals, alkaline-earth metals, and lanthanides (a), of transition metals (b), and of metalloids and post-transition metals (c) on IIP (solid) and NIP (hatched) V. P: percolation of 1 mL of 25 mM Bis-Tris buffer at pH 7 spiked with 0.01 Bq mL^{-1} of $^{226}Ra(II)$ and 10 µg L^{-1}

of other elements. W: washing with 0.5 mL of UP water and 0.5 mL of HNO_3 pH 4. E1 to E3: Elution with 0.5 mL of HNO_3 pH 3, 0.5 mL of HNO_3 pH 2, and 1.5 mL of HNO_3 0.5 M, respectively. All fractions were analyzed with an ICP-QQQ-MS (Agilent 8800). Oxidation degrees assumed to be predominant between pH 1 and 7. The presented data are from one SPE.

Some of the main competitors identified, such as Bi, Pb, Ba, and Sr that are retained by the IIP, can form polyatomic interferences in ICP-MS. The formation of spectral interferences actually depends on several factors including interfering element concentration, the type of introduction system and ICP-MS employed, as well as the analysis settings (gas rates, resolution, MS/MS, use of the collision reaction cell). We examined here from which concentration they induced an apparent signal at *m/z* 226 (mass followed for ^{226}Ra measurement) on our measurement system: Apex Omega hyphenated to an ICP-QQQ-MS Agilent 8800 operated in MS mode. The formation of oxide- and hydroxide-based polyatomic interferences was expected to be minimized using such introduction system. However, as shown in Figure S10, main interferences arise from the presence of Bi ($^{209}Bi^{16}O^{1}H^{+}$ and $^{209}Bi^{17}O^{+}$) and W ($^{40}Ar^{186}W^{+}$) whose signals start to be significant (≥ 1 CPS, background signal measured in a 0.5 M HNO_3 blank solution) from 20 and 60 µg L^{-1}, respectively. Impact of Pb ($^{208}Pb^{18}O^{+}$ and $^{209}Pb^{16}O^{1}H_2^{+}$) and Sr/Ba ($^{88}Sr^{138}Ba^{+}$) solutions was minor, even at high concentrations (>200 µg L^{-1}). Aforementioned observations are in agreement with results obtained in another study using the same instrument (introduction system not specified) [6]. Working on an iCAP-Q ICP-MS, Ben Yaala *et al.* remarked these elements were also the most disrupting but concentrations from which they induced a signal at *m/z* 226 was lower (e.g. 2 and 5 µg L^{-1} for Bi and W, respectively) [61]. W is not retained on the IIP and should not be present in the analyzed fraction, but concerning the other elements, it will be necessary to know their concentration in real samples to see if a mathematical correction needs to be made to take into account their contribution at *m/z* 226. For instance, their average abundances in the earth's crust are as follows but are expected to be lower in environmental waters: 0.1 (Bi), 10 (Pb), and 100 mg kg^{-1} (Sr, Ba) [62].

3.3.2. SPE procedure optimization trials for specificity improvement

To avoid manipulating radioactive sources in this development phase, Ba(II) was again used as representative of Ra(II). To limit the co-extraction of interfering ions such as Sr(II), La(III), Co(II), and Pb(II) with Ba(II), modifications of the SPE procedure were attempted. The various assays are summarized in Table S11. In the first trial, Bis-Tris concentration in the first washing step was increased (from 25 to 200 mM) to reduce the retention of some competitors. Results obtained with 25 mM of Bis-Tris were comparable to those observed employing UP water, and for higher concentrations, all ions were slightly less retained on the support and still co-extracted. Since under the conditions of Figure 3, ions were eluted between pH 3 and 2 (cf fractions E1+E2), the effect of applying a more gradual pH decrease (in steps of 0.5) on ion retention was studied. However, this did not have more discriminatory impact, even by further reducing the pH decrement. Subsequently, the influence of loading the sample at pH 4 was also assessed. It led to a loss of retention for all ions, which can be explained by the protonation of the acid moieties present in cavities at this pH. Finally, a significant improvement could be obtained by playing on the volume of elution solution at pH 4. Indeed, after loading the sample at pH 6 fixed with HNO_3 and applying a first washing step with 0.5 mL of UP water, 5 mL of HNO_3 at pH 4 were passed through cartridges. Collection of fractions every 0.5 mL revealed that in these conditions, Ba(II) and Sr(II) are co-extracted in fractions E1 and E2 (20% and 70% of the total recovery, respectively) while La(III) is eluted in fractions E2 (up to 40%) to E11, and most part of Pb(II) falls into fraction E11 (Figure 4). This allowed to remove a part of La(III) and Pb(II) interferences.

It is worthwhile to notice that at least 20 extractions were made using the same sorbent without observing any drop in performance. In our mind, the IIP V is a promising sorbent enabling the extraction of Ba(II), a strong analogue of Ra(II). It should be more interesting to assess in the future if varying synthesis parameters such as the template/monomer or the template/co-monomer/cross-linker ratios can enhance the intrinsic specificity of the support rather than testing other extraction conditions. Determining the capacity, breakthrough volume, and synthesis repeatability is thus not primordial at this stage.

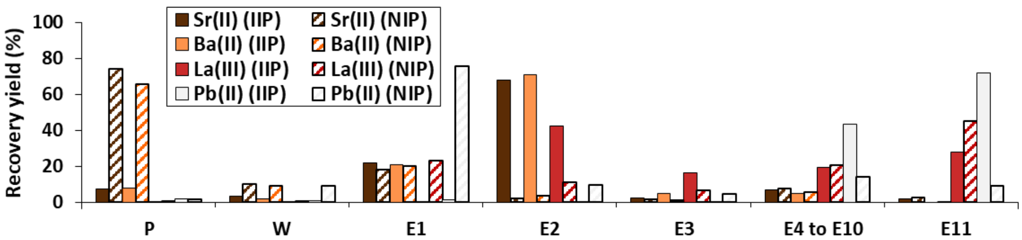

Figure 4: Best SPE profile after optimization trials on IIP and NIP V playing on volume of elution solution. P: percolation of 1 mL of HNO_3 at pH 6 spiked with 15 µg L^{-1} of Ba(II), and Sr(II), and with 10 µg L^{-1} of La(III), and Pb(II). W: washing with 0.5 mL of UP water. E1 to E10: Elution with 10 x 0.5 mL of HNO_3 pH 4. E11: Elution with 3 mL of HNO_3 0.5 M. All fractions were analyzed with an ICP-(CC)-Q-MS system (Agilent 7700x). The presented data ensue from one SPE.

4. Conclusion

The objective of this work was to assess, for the first time, the possibility to design an IIP for the extraction of Ra(II). Due to the poor background in literature concerning IIP for alkaline earth metal, a complete screening approach was implemented to rationalize the selection of functional monomers, template/monomer ratios, and complexation times. ESI-MS and conductimetry proved to be relevant prediction techniques though they have never been used in this context before. Among the five IIPs/NIPs synthesized in ACN/DMSO (1/1, v/v), IIP V, resulting from the use of Ba(II) as template ion, VPA and styrene as monomer and co-monomer, and DVB as cross-linker, with a molar ratio of 1/6/20/20, was able to selectively extract Ra(II) and had no affinity for alkalis and some other metals (V, Mo, W, As, Sb, etc).

Main constraint encountered during syntheses was the limited choice of porogen due to the poor solubility of $Ba(NO_3)_2$ salt in a low volume of organic solvent. In addition, the VPA-based IIP (IIP V) showed only a partial specificity even after several SPE procedure optimization trials. There are opportunities to improve this aspect by changing the template/monomers or the template/co-monomer/cross-linker ratios. Comparing the performances in terms of specificity, capacity, breakthrough volume of these new syntheses constitutes the main perspective of this work which has already given very encouraging results and opens up the possibility of applying IIP for the extraction of radium in real samples.

Acknowledgements

The authors thank the Institute of Porous MAterials of Paris (IMAP), a joint CNRS-ENS-ESPCI laboratory, for having allowed them to perform thermogravimetric analyses on their instrument, and Gilles Alcade (IRSN) for providing his help during BET experiments. This is PATERSON, the IRSN mass spectrometry platform, contribution n°14.

References

[1] International Atomic Energy Agency, The environmental behaviour of radium, 2014.

[2] P. Thakur, A.L. Ward, A.M. González-Delgado, Optimal methods for preparation, separation, and determination of radium isotopes in environmental and biological samples, J. Environ. Radioact. 228 (2021) 106522. https://doi.org/10.1016/j.jenvrad.2020.106522.

[3] M. Boudias, A. Gourgiotis, G. Montavon, C. Cazala, V. Pichon, N. Delaunay, 226Ra and 137Cs determination by inductively coupled plasma mass spectrometry: state of the art and perspectives including sample pretreatment and separation steps, J. Environ. Radioact. 244–245 (2022) 106812. https://doi.org/10.1016/j.jenvrad.2022.106812.

[4] M. Bonin, D. Larivière, P.P. Povinec, Detection of radium at the attogram per gram level in copper by inductively coupled plasma mass spectrometry after cation-exchange chromatography, Anal. Methods. 12 (2020) 2272–2278. https://doi.org/10.1039/D0AY00512F.

[5] G. Yang, J. Zheng, K. Tagami, S. Uchida, J. Zhang, J. Wang, J. Du, Simple and sensitive determination of radium-226 in river water by single column-chromatographic separation coupled to SF-ICP-MS analysis in medium resolution mode, J. Environ. Radioact. 220–221 (2020) 106305. https://doi.org/10.1016/j.jenvrad.2020.106305.

[6] C. Dalencourt, A. Michaud, A. Habibi, A. Leblanc, D. Larivière, Rapid, versatile and sensitive method for the quantification of radium in environmental samples through cationic extraction and inductively coupled plasma mass spectrometry, J. Anal. At. Spectrom. 33 (2018) 1031–1040. https://doi.org/10.1039/C8JA00060C.

[7] E.M. van Es, B.C. Russell, P. Ivanov, D. Read, Development of a method for rapid analysis of Ra-226 in groundwater and discharge water samples by ICP-QQQ-MS, Appl. Radiat. Isot. 126 (2017) 31–34. https://doi.org/10.1016/j.apradiso.2017.02.019.

[8] W. Wang, R.D. Evans, K. Newman, A. Toms, Automated separation and measurement of 226Ra and trace metals in freshwater, seawater and fracking water by online ion exchange chromatography coupled with ICP-MS, Microchem. J. 167 (2021) 106321. https://doi.org/10.1016/j.microc.2021.106321.

[9] T. Zhang, D. Bain, R. Hammack, R.D. Vidic, Analysis of Radium-226 in High Salinity Wastewater from Unconventional Gas Extraction by Inductively Coupled Plasma-Mass Spectrometry, Environ. Sci. Technol. 49 (2015) 2969–2976. https://doi.org/10.1021/es504656q.

[10] F. Lagacé, D. Foucher, C. Surette, O. Clarisse, Quantification of 226Ra at environmental relevant levels in natural waters by ICP-MS: Optimization, validation and limitations of an extraction and preconcentration approach, Talanta. 167 (2017) 658–665. https://doi.org/10.1016/j.talanta.2017.02.031.

[11] R.D. Evans, A. Izmer, K. Benkhedda, A. Toms, A. Fernando, W. Wang, Continuous online determination of ^{226}Ra in liquid effluents using automated column chromatography-ICP-MS, Can. J. Chem. 93 (2015) 1226–1231. https://doi.org/10.1139/cjc-2015-0247.

[12] L. Copia, S. Nisi, W. Plastino, M. Ciarletti, P.P. Povinec, Low-level 226Ra determination in groundwater by SF-ICP-MS: optimization of separation and pre-concentration methods, J. Anal. Sci. Technol. 6 (2015) 22. https://doi.org/10.1186/s40543-015-0062-5.

[13] D. Larivière, D.K. Brownell, V.N. Epov, R.J. Cornett, R.D. Evans, Determination of 226Ra in sediments by ICP-MS: A comparative study of three sample preparation approaches, J. Radioanal. Nucl. Chem. 273 (2007) 337–344. https://doi.org/10.1007/s10967-007-6870-3.

[14] D. Larivière, V.N. Epov, K.M. Reiber, R.J. Cornett, R.D. Evans, Micro-extraction procedures for the determination of Ra-226 in well waters by SF-ICP-MS, Anal. Chim. Acta. 528 (2005) 175–182. https://doi.org/10.1016/j.aca.2004.09.076.

[15] C. Dalencourt, M.N. Chabane, J.-C. Tremblay-Cantin, D. Larivière, A rapid sequential chromatographic separation of U- and Th-decay series radionuclides in water samples, Talanta. 207 (2020) 120282. https://doi.org/10.1016/j.talanta.2019.120282.

[16] M. Verlinde, J. Gorny, G. Montavon, S. Khalfallah, B. Boulet, C. Augeray, D. Larivière, C. Dalencourt, A. Gourgiotis, A new rapid protocol for 226Ra separation and preconcentration in natural water samples using molecular recognition technology for ICP-MS analysis, J. Environ. Radioact. 202 (2019) 1–7. https://doi.org/10.1016/j.jenvrad.2019.02.003.

[17] F. Shakerian, K.-H. Kim, E. Kwon, J.E. Szulejko, P. Kumar, S. Dadfarnia, A.M. Haji Shabani, Advanced polymeric materials: Synthesis and analytical application of ion imprinted polymers as selective sorbents for solid phase extraction of metal ions, TrAC Trends Anal. Chem. 83 (2016) 55–69. https://doi.org/10.1016/j.trac.2016.08.001.

[18] C. Branger, W. Meouche, A. Margaillan, Recent advances on ion-imprinted polymers, React. Funct. Polym. 73 (2013) 859–875. https://doi.org/10.1016/j.reactfunctpolym.2013.03.021.

[19] Y. El Ouardi, A. Giove, M. Laatikainen, C. Branger, K. Laatikainen, Benefit of ion imprinting technique in solid-phase extraction of heavy metals, special focus on the last decade, J. Environ. Chem. Eng. 9 (2021) 106548. https://doi.org/10.1016/j.jece.2021.106548.

[20] V.V. Kusumkar, M. Galamboš, E. Viglašová, M. Daňo, J. Šmelková, Ion-Imprinted Polymers: Synthesis, Characterization, and Adsorption of Radionuclides, Mater. Basel Switz. 14 (2021) 1083. https://doi.org/10.3390/ma14051083.

[21] R.D. Shannon, Revised effective ionic radii and systematic studies of interatomic distances in halides and chalcogenides, Acta Crystallogr. Sect. A. 32 (1976) 751–767. https://doi.org/10.1107/S0567739476001551.

[22] M. Dudev, J. Wang, T. Dudev, C. Lim, Factors Governing the Metal Coordination Number in Metal Complexes from Cambridge Structural Database Analyses, J. Phys. Chem. B. 110 (2006) 1889–1895. https://doi.org/10.1021/jp054975n.

[23] H. Sid Kalal, N. Pakizevand, H. Hoveidi, M. Taghiof, S. Tavangari, H. Ahmad Panahi, Adsorption of Strontium (II) on new ion-imprinted solid-phase support: determination, isotherms, thermodynamic and kinetic studies, Casp. J. Environ. Sci. 11 (2013) 53–63.

[24] C. Li, X. Zhang, J. Pan, P. Xu, Y. Liu, Y. Yan, Z. Zhang, Strontium(II) Ion Surface-Imprinted Polymers Supported by Potassium Tetratitanate Whiskers: Synthesis, Characterization and Adsorption Behaviours, Adsorpt. Sci. Technol. 27 (2009) 845–859. https://doi.org/10.1260/0263-6174.27.9.845.

[25] Q. Li, H. Liu, T. Liu, M. Guo, B. Qing, X. Ye, Z. Wu, Strontium and calcium ion adsorption by molecularly imprinted hybrid gel, Chem. Eng. J. 157 (2010) 401–407. https://doi.org/10.1016/j.cej.2009.11.029.

[26] Y. Liu, R. Chen, D. Yuan, Z. Liu, M. Meng, Y. Wang, J. Han, X. Meng, F. Liu, Z. Hu, W. Guo, L. Ni, Y. Yan, Thermal-responsive ion-imprinted polymer based on magnetic mesoporous silica SBA-15 for selective removal of Sr(II) from aqueous solution, Colloid Polym. Sci. 293 (2015) 109–123. https://doi.org/10.1007/s00396-014-3393-7.

[27] Y. Liu, J. Gao, Z. Zhang, J. Dai, J. Xie, Y. Yan, A New Sr(II) Ion-Imprinted Polymer Grafted onto Potassium Titanate Whiskers: Synthesis and Adsorption Performance for the Selective

Separation of Strontium Ions, Adsorpt. Sci. Technol. 28 (2010) 23–37. https://doi.org/10.1260/0263-6174.28.1.23.

[28] Y. Liu, F. Liu, L. Ni, M. Meng, X. Meng, G. Zhong, J. Qiu, A modeling study by response surface methodology (RSM) on Sr(II) ion dynamic adsorption optimization using a novel magnetic ion imprinted polymer, RSC Adv. 6 (2016) 54679–54692. https://doi.org/10.1039/C6RA07270D.

[29] Y. Liu, X. Meng, M. Luo, M. Meng, L. Ni, J. Qiu, Z. Hu, F. Liu, G. Zhong, Z. Liu, Y. Yan, Synthesis of hydrophilic surface ion-imprinted polymer based on graphene oxide for removal of strontium from aqueous solution, J. Mater. Chem. A. 3 (2015) 1287–1297. https://doi.org/10.1039/C4TA04908J.

[30] J. Pan, X. Zou, Y. Yan, X. Wang, W. Guan, J. Han, X. Wu, An ion-imprinted polymer based on palygorskite as a sacrificial support for selective removal of strontium(II), Appl. Clay Sci. 50 (2010) 260–265. https://doi.org/10.1016/j.clay.2010.08.007.

[31] Y. Song, H. Ou, W. Bian, Y. Zhang, J. Pan, Y. Liu, W. Huang, Ion-Imprinted Polymers Based on Hollow Silica with Yeasts as Sacrificial Supports for Sr2+ Selective Adsorption, J. Inorg. Organomet. Polym. Mater. 23 (2013) 1325–1334. https://doi.org/10.1007/s10904-013-9927-5.

[32] Z. Zhang, L. Li, Synthesis and characterization of whisker surface imprinted polymer and selective solid-phase extraction of trace Sr(II) from environment aqueous solution, Desalination Water Treat. 54 (2015) 2441–2451. https://doi.org/10.1080/19443994.2014.899926.

[33] T. Rosatzin, L.I. Andersson, W. Simon, K. Mosbach, Preparation of Ca2+ selective sorbents by molecular imprinting using polymerisable ionophores, J. Chem. Soc. Perkin Trans. 2. (1991) 1261–1265. https://doi.org/10.1039/P29910001261.

[34] Y. Ben-Amram, R. Tel-Vered, M. Riskin, Z.-G. Wang, I. Willner, Ultrasensitive and selective detection of alkaline-earth metal ions using ion-imprinted Au NPs composites and surface plasmon resonance spectroscopy, Chem Sci. 3 (2012) 162–167. https://doi.org/10.1039/C1SC00403D.

[35] M. Moussa, V. Pichon, C. Mariet, T. Vercouter, N. Delaunay, Potential of ion imprinted polymers synthesized by trapping approach for selective solid phase extraction of lanthanides, Talanta. 161 (2016) 459–468. https://doi.org/10.1016/j.talanta.2016.08.069.

[36] C. Ni, Q. Liu, Z. Ren, H. Hu, B. Sun, C. Liu, P. Shao, L. Yang, S.G. Pavlostathis, X. Luo, Selective removal and recovery of La(III) using a phosphonic-based ion imprinted polymer: Adsorption performance, regeneration, and mechanism, J. Environ. Chem. Eng. 9 (2021) 106701. https://doi.org/10.1016/j.jece.2021.106701.

[37] M. Yolcu, N. Dere, A novel copper selective sensor based on ion imprinted 2-vinylpyridine polymer, Can. J. Chem. 96 (2018) 1027–1036. https://doi.org/10.1139/cjc-2018-0178.

[38] F.W.B. van Leeuwen, W. Verboom, D.N. Reinhoudt, Selective extraction of naturally occurring radioactive Ra2+, Chem. Soc. Rev. 34 (2005) 753. https://doi.org/10.1039/b506073g.

[39] K. Karim, F. Breton, R. Rouillon, E. Piletska, A. Guerreiro, I. Chianella, S. Piletsky, How to find effective functional monomers for effective molecularly imprinted polymers?, Adv. Drug Deliv. Rev. 57 (2005) 1795–1808. https://doi.org/10.1016/j.addr.2005.07.013.

[40] R.L.M. Mesa, J.E.L. Villa, S. Khan, R.R.A. Peixoto, M.A. Morgano, L.M. Gonçalves, M.D.P.T. Sotomayor, G. Picasso, Rational Design of an Ion-Imprinted Polymer for Aqueous Methylmercury Sorption, Nanomaterials. 10 (2020) 2541. https://doi.org/10.3390/nano10122541.

[41] Z. Liu, Z. Xu, D. Wang, Y. Yang, Y. Duan, L. Ma, T. Lin, H. Liu, A review on molecularly imprinted polymers preparation by computational simulation-aided methods, Polymers. 13 (2021) 2657. https://doi.org/10.3390/polym13162657.

[42] M.L. Dietz, R. Chiarizia, E.P. Horwitz, R.A. Bartsch, V. Talanov, Effect of Crown Ethers on the Ion-Exchange Behavior of Alkaline Earth Metals. Toward Improved Ion-Exchange Methods for the Separation and Preconcentration of Radium, Anal. Chem. 69 (1997) 3028–3037. https://doi.org/10.1021/ac9700437.

[43] J. Kupai, M. Razali, S. Buyuktiryaki, R. Kecili, G. Szekely, Long-term stability and reusability of molecularly imprinted polymers, Polym. Chem. 8 (2017) 666–673. https://doi.org/10.1039/C6PY01853J.

[44] D.K. Singh, S. Mishra, Synthesis and characterization of Fe(III)-ion imprinted polymer for recovery of Fe(III) from water samples, J. Sci. Ind. Res. 69 (2010). http://nopr.niscair.res.in/handle/123456789/10300.

[45] S. Shirvani-Arani, S.J. Ahmadi, A. Bahrami-Samani, M. Ghannadi-Maragheh, Synthesis of nano-pore samarium (III)-imprinted polymer for preconcentrative separation of samarium ions from other lanthanide ions via solid phase extraction, Anal. Chim. Acta. 623 (2008) 82–88. https://doi.org/10.1016/j.aca.2008.05.071.

[46] S.J. Ahmadi, O. Noori-Kalkhoran, S. Shirvani-Arani, Synthesis and characterization of new ion-imprinted polymer for separation and preconcentration of uranyl (UO22+) ions, J. Hazard. Mater. 175 (2010) 193–197. https://doi.org/10.1016/j.jhazmat.2009.09.148.

[47] M. Gawin, J. Konefał, B. Trzewik, S. Walas, A. Tobiasz, H. Mrowiec, E. Witek, Preparation of a new Cd(II)-imprinted polymer and its application to determination of cadmium(II) via flow-injection-flame atomic absorption spectrometry, Talanta. 80 (2010) 1305–1310. https://doi.org/10.1016/j.talanta.2009.09.021.

[48] Q.O. dos Santos, M.A. Bezerra, G. de F. Lima, K.M. Diniz, M.G. Segatelli, T.O. Germiniano, V. da S. Santos, C.R.T. Tarley, Synthesis, characterization and application of ion imprinted poly(vinylimidazole) for zinc ion extraction/preconcentration with FAAS determination, Quím. Nova. 37 (2014) 63–68. https://doi.org/10.1590/S0100-40422014000100012.

[49] F. Mehamod, N.F. Yusof, N. Jusoh, M. Abdul Kadir, F.B. Mohd Suah, Synthesis and Adsorption Studies for Newly Prepared Ni2+-imprinted Polymer co-Functionalized with Picolinic Acid, ASM Sci. J. Special issue (2018) 114–123.

[50] H.-G. Wu, X.-J. Ju, R. Xie, Y.-M. Liu, J.-G. Deng, C.H. Niu, L.-Y. Chu, A novel ion-imprinted hydrogel for recognition of potassium ions with rapid response, Polym. Adv. Technol. 22 (2011) 1389–1394. https://doi.org/10.1002/pat.1843.

[51] M. Khajeh, M. Kaykhaii, M. Mirmoghaddam, H. Hashemi, Separation of zinc from aqueous samples using a molecular imprinting technique, Int. J. Environ. Anal. Chem. 89 (2009) 981–992. https://doi.org/10.1080/03067310902719159.

[52] R. Kala, T.P. Rao, Ion imprinted polymer particles for separation of yttrium from selected lanthanides, J. Sep. Sci. 29 (2006) 1281–1287. https://doi.org/10.1002/jssc.200600008.

[53] N. Behnia, M. Asgari, A. Feizbakhsh, Sub-nanomolar detection of zinc on the ion-imprinted polymer modified glassy carbon electrode, J. Environ. Chem. Eng. 3 (2015) 271–276. https://doi.org/10.1016/j.jece.2014.11.008.

[54] M.R.R. Kahkha, M. Kaykhaii, Determination and extraction of zinc from aqueous solution using ion-imprinted polymer., Int. Res. J. Appl. Basic Sci. 8 (2014) 707–711.

[55] F. Shakerian, S. Dadfarnia, A.M.H. Shabani, Synthesis and application of nano-pore size ion imprinted polymer for solid phase extraction and determination of zinc in different matrices, Food Chem. 134 (2012) 488–493. https://doi.org/10.1016/j.foodchem.2012.02.105.

[56] F. Xie, G. Liu, F. Wu, G. Guo, G. Li, Selective adsorption and separation of trace dissolved Fe(III) from natural water samples by double template imprinted sorbent with chelating diamines, Chem. Eng. J. 183 (2012) 372–380. https://doi.org/10.1016/j.cej.2012.01.018.

[57] M. Mitreva, I. Dakova, I. Karadjova, Iron(II) ion imprinted polymer for Fe(II)/Fe(III) speciation in wine, Microchem. J. 132 (2017) 238–244. https://doi.org/10.1016/j.microc.2017.01.023.

[58] M.C. Burleigh, S. Dai, E.W. Hagaman, J.S. Lin, Imprinted Polysilsesquioxanes for the Enhanced Recognition of Metal Ions, Chem. Mater. 13 (2001) 2537–2546. https://doi.org/10.1021/cm000894m.

[59] M. Behbahani, M. Salarian, A. Bagheri, H. Tabani, F. Omidi, A. Fakhari, Synthesis, characterization and analytical application of Zn(II)-imprinted polymer as an efficient solid-phase extraction technique for trace determination of zinc ions in food samples, J. Food Compos. Anal. 34 (2014) 81–89. https://doi.org/10.1016/j.jfca.2013.10.003.

[60] M. Randhawa, I. Gartner, C. Becker, J. Student, M. Chai, A. Mueller, Imprinted polymers for water purification, J. Appl. Polym. Sci. 106 (2007) 3321–3326. https://doi.org/10.1002/app.26873.

[61] H. Ben Yaala, R. Fniter, D. Foucher, O. Clarisse, Direct analysis of radium-226 in sediment by ICP-MS: an analytical challenge?, J. Anal. At. Spectrom. 34 (2019) 1597–1605. https://doi.org/10.1039/C9JA00156E.

[62] A.G. Darnley, A. Bjoerklund, B. Boelviken, N. Gustavsson, P.V. Koval, J.A. Plant, A. Steenfelt, M. Tauchid, X. Xie, A global geochemical database for environmental and resource management. Recommendations for international geochemical mapping final report of IGCP project 259, UNESCO, 1995.

Table S1: ICP-MS acquisition parameters. Tl was only used as internal standard (IS) for some experiments.

	Agilent 7700x	**Agilent 8800**
Isotopes monitored	^{133}Cs, ^{138}Ba, (IS: ^{205}Tl)	^{7}Li, ^{85}Rb, ^{133}Cs, ^{88}Sr, ^{137}Ba, ^{226}Ra, ^{139}La, ^{51}V, ^{59}Co, ^{93}Nb, ^{95}Mo, ^{107}Ag, ^{182}W, ^{75}As, ^{121}Sb, ^{205}Tl, ^{208}Pb, ^{209}Bi, ^{232}Th, ^{238}U
Peak pattern	1 point	1 point
Integration time (s)	0.3 for all *m/z*	2 for *m/z* 226, 0.05 for all other *m/z*
Number of replicates	5	4
Number of sweeps	100	100

Table S2: Species observed in ESI(+)-MS for a mixture of barium nitrate and DEGDE as ligand (L) with molar ratios 1/1 (m/z_{exp} A) and 1/6 (m/z_{exp} B) after a short complexation time, and with ratios 1/1 (m/z_{exp} C) and 1/6 (m/z_{exp} D) after a long complexation time. In parentheses is indicated in which case the specie was observed. Data treatment was realized on one infusion.

Average m/z_{exp} ± 2σ	**m/z_{theo}**	**Molecular formula**	**Observed specie**	**Error (ppm)**
		ESI(+)		
159.1019 ± 0.0002 (A, B, C, D)	159.1021	$C_8H_{15}O_3$	$[L+H]^+$	1.57
227.0465 ± 0.0003 (A, B, C, D)	227.0469	$C_{16}H_{28}O_6Ba$	$[Ba+2L]^{2+}$	1.76
306.0938 ± 0.0004 (A, B, C, D)	306.0941	$C_{24}H_{42}O_9Ba$	$[Ba+3L]^{2+}$	0.98

Table S3: Species observed in ESI(+/-)-MS for a mixture of barium nitrate and MAA as ligand (L) with molar ratios 1/1 (m/z_{exp} A) and 1/6 (m/z_{exp} B) after a short complexation time, and with ratios 1/1 (m/z_{exp} C) and 1/6 (m/z_{exp} D) after a long complexation time. In parentheses is indicated in which case the specie was observed. *: Signal was not continuous over the entire infusion period. Data treatment was realized on one infusion.

Average m/z_{exp} ± 2σ	**m/z_{theo}**	**Molecular formula**	**Observed specie**	**Error (ppm)**
		ESI(+)		
87.0448 ± 0 (A, B, C, D)	87.0446	$C_4H_7O_2$	$[L+H]^+$	2.3
222.9340 ± 0.0002 (A, B, C, D)	222.9342	$C_4H_5O_2Ba$	$[Ba+L-H]^+$	0.9
308.9707 ± 0.0003 (A, B, C, D)	308.9710	$C_8H_{11}O_4Ba$	$[Ba+2L-H]^+$	0.9
395.0079 ± 0.0004 (A, B, C, D)	395.0078	$C_{12}H_{17}O_6Ba$	$[Ba+3L-H]^+$	0.1
481.0447 ± 0.0004 (A*, B, D)	481.0445	$C_{16}H_{23}O_8Ba$	$[Ba+4L-H]^+$	0.4
		ESI(-)		
392.9924 ± 0.0004 (A, B, C, D)	392.9921	$C_{12}H_{15}O_6Ba$	$[Ba+3L-3H]^-$	0.8

Table S4: Species observed in ESI(+)-MS for a mixture of barium nitrate and 2-VP as ligand (L) with molar ratios 1/1 (m/z_{exp} A) and 1/6 (m/z_{exp} B) after a short complexation time, and with ratios 1/1 (m/z_{exp} C) and 1/6 (m/z_{exp} D) after a long complexation time. In parentheses is indicated in which case the specie was observed. Data treatment was realized on one infusion.

Average $m/z_{exp} \pm 2\sigma$	m/z_{theo}	Molecular formula	Observed specie	Error (ppm)
		ESI(+)		
106.0659 ± 0.0001 (C, D)	106.0657	C_7H_8N	$[L+H]^+$	1.4
226.5385 (D)	226.5394	$C_{21}H_{21}N_3Ba$	$[Ba+3L]^{2+}$	4.0

Table S5: Species observed in ESI(+)-MS for a mixture of barium nitrate and VPA as ligand (L) with molar ratios 1/1 (m/z_{exp} A) and 1/6 (m/z_{exp} B) after a short complexation time, and with ratios 1/1 (m/z_{exp} C) and 1/6 (m/z_{exp} D) after a long complexation time. In parentheses is indicated in which case the specie was observed. *: Signal was not continuous over the entire infusion period. Data treatment was realized on one infusion.

Average m/z_{exp} ± 2σ	m/z_{theo}	Molecular formula	Observed specie	Error (ppm)
		ESI(+)		
109.0056 ± 0.0001 (A, B, C, D)	109.0055	$C_2H_6O_3P$	$[L+H]^+$	0.9
244.8948 ± 0.0008 (A, B, C, D)	244.8951	$C_2H_4O_3PBa$	$[Ba+L-H]^+$	1.2
352.8927 ± 0.0003 (A, B, C, D)	352.8927	$C_4H_9O_6P_2Ba$	$[Ba+2L-H]^+$	0.1
460.8907 ± 0.0003 (A*, B, C*, D)	460.8903	$C_6H_{14}O_9P_3Ba$	$[Ba+3L-H]^+$	0.9
568.8886 ± 0.0005 (B*, D)	568.8879	$C_8H_{19}O_{12}P_4Ba$	$[Ba+4L-H]^+$	1.1
676.8867 ± 0.0005 (C*, D*)	676.8856	$C_{10}H_{24}O_{15}P_5Ba$	$[Ba+5L-H]^+$	1.6
784.8843 (D*)	784.8832	$C_{12}H_{29}O_{18}P_6Ba$	$[Ba+6L-H]^+$	1.4

Table S6: Species observed in ESI(+/-)-MS for a mixture of barium nitrate, DEGDE as first ligand (L1), and MAA as second ligand (L2) in proportions 1/4/3 (molar ratio) after a short complexation time (m/z_{exp} A), and after a long complexation time (m/z_{exp} B). In parentheses is indicated in which case the specie was observed. *: Signal was not continuous over the entire infusion period. Data treatment was realized on one infusion.

Average m/z_{exp} ± 2σ	**m/z_{theo}**	**Molecular formula**	**Observed specie**	**Error (ppm)**
		ESI(+)		
87.0449 ± 0.0001 (A, B)	87.0446	$C_4H_7O_2$	$[L2+H]^+$	2.9
147.9987 (B*)	147.9998	$C_8H_{14}O_3Ba$	$[Ba+L1]^{2+}$	7.1
159.1021 ± 0.0001 (A, B)	159.1021	$C_8H_{15}O_3$	$[L1+H]^+$	0.3
191.0178 (A*)	191.0182	$C_{12}H_{20}O_5Ba$	$[Ba+L1+L2]^{2+}$	1.8
222.9342 ± 0 (A, B)	222.9342	$C_4H_5O_2Ba$	$[Ba+L2-H]^+$	0.0
227.0468 ± 0.0003 (A, B)	227.0469	$C_{16}H_{28}O_6Ba$	$[Ba+2L1]^{2+}$	0.7
270.0650 (A*)	270.0653	$C_{20}H_{34}O_8Ba$	$[Ba+2L1+L2]^{2+}$	1.1
306.0939 ± 0.0001 (A, B)	306.0941	$C_{24}H_{42}O_9Ba$	$[Ba+3L1]^{2+}$	0.7
308.9707 ± 0.0001 (A, B)	308.9710	$C_8H_{11}O_4Ba$	$[Ba+2L2-H]^+$	1.1
313.0833 (A*)	313.0837	$C_{24}H_{40}O_{10}Ba$	$[Ba+2L1+2L2]^{2+}$	1.3
349.1122 (A*)	349.1125	$C_{28}H_{48}O_{11}Ba$	$[Ba+3L1+L2]^{2+}$	0.7
381.0285 ± 0.0003 (A, B)	381.0285	$C_{12}H_{19}O_5Ba$	$[Ba+L1+L2-H]^+$	0.1
395.0079 ± 0.0003 (A, B)	395.0078	$C_{12}H_{17}O_6Ba$	$[Ba+3L2-H]^+$	0.1
539.1232 ± 0.0003 (A, B)	539.1228	$C_{20}H_{33}O_8Ba$	$[Ba+2L1+L2-H]^+$	1.0
553.1024 (A*)	553.1021	$C_{20}H_{31}O_9Ba$	$[Ba+L1+3L2-H]^+$	0.5
625.1603 ± 0.0002 (A*, B*)	625.1596	$C_{24}H_{39}O_{10}Ba$	$[Ba+2L1+2L2-H]^+$	1.1
		ESI(-)		
392.9922 ± 0 (A, B)	392.9921	$C_{12}H_{15}O_6Ba$	$[Ba+3L2-3H]^-$	0.3

Table S7: Species observed in ESI(+)-MS for a mixture of barium nitrate, DEGDE as first ligand (L1), and 2-VP as second ligand (L2) in proportions 1/4/3 (molar ratio) after a short complexation time (m/z_{exp} A), and after a long complexation time (m/z_{exp} B). In parentheses is indicated in which case the specie was observed. *: Signal was not continuous over the entire infusion period. Data treatment was realized on one infusion.

Average m/z_{exp} ± 2σ	**m/z_{theo}**	**Molecular formula**	**Observed specie**	**Error (ppm)**
		ESI(+)		
106.0660 ± 0.0002 (A, B)	106.0657	C_7H_8N	$[L2+H]^+$	2.4
159.1021 ± 0.0001 (A, B)	159.1021	$C_8H_{15}O_3$	$[L1+H]^+$	0.3
227.0468 ± 0.0001 (A, B)	227.0469	$C_{16}H_{28}O_6Ba$	$[Ba+2L1]^{2+}$	0.7
253.0575 (A*)	253.0576	$C_{22}H_{28}O_3N_2Ba$	$[Ba+L1+2L2]^{2+}$	0.4
306.0941 ± 0.0002 (A, B)	306.0941	$C_{24}H_{42}O_9Ba$	$[Ba+3L1]^{2+}$	0.2

Table S8: Species observed in ESI(+)-MS for a mixture of barium nitrate, DEGDE as first ligand (L1), and VPA as second ligand (L2) in proportions 1/4/3 (molar ratio) after a short complexation time (m/z_{exp} A), and after a long complexation time (m/z_{exp} B). In parentheses is indicated in which case the specie was observed. *: Signal was not continuous over the entire infusion period. Data treatment was realized on one infusion.

Average $m/z_{exp} \pm 2\sigma$	m/z_{theo}	Molecular formula	Observed specie	Error (ppm)
		ESI(+)		
109.0056 ± 0.0001 (A, B)	109.0055	$C_2H_6O_3P$	$[L2+H]^+$	0.5
147.9990 (A*)	147.9998	$C_8H_{14}O_3Ba$	$[Ba+L1]^{2+}$	5.1
159.1020 ± 0.0001 (A, B)	159.1021	$C_8H_{15}O_3$	$[L1+H]^+$	0.9
227.0466 ± 0.0004 (A, B)	227.0469	$C_{16}H_{28}O_6Ba$	$[Ba+2L1]^{2+}$	1.3
244.8946 ± 0.0005 (A, B)	244.8951	$C_2H_4O_3PBa$	$[Ba+L2-H]^+$	2.3
281.0457 (A*)	281.0458	$C_{18}H_{33}O_9PBa$	$[Ba+2L1+L2]^{2+}$	0.2
306.0938 ± 0.0004 (A, B*)	306.0941	$C_{24}H_{42}O_9Ba$	$[Ba+3L1]^{2+}$	0.8
352.8926 ± 0.0005 (A, B)	352.8927	$C_4H_9O_6P_2Ba$	$[Ba+2L2-H]^+$	0.4
385.1416 (A*)	385.1412	$C_{32}H_{56}O_{12}Ba$	$[Ba+4L1]^{2+}$	1.0
402.9897 (A)	402.9893	$C_{10}H_{18}O_6PBa$	$[Ba+L1+L2-H]^+$	1.0
510.9877 (A*)	510.9870	$C_{12}H_{23}O_9P_2Ba$	$[Ba+L1+2L2-H]^+$	1.4
561.0841 ± 0.0010 (A*, B)	561.0836	$C_{18}H_{32}O_9PBa$	$[Ba+2L1+L2-H]^+$	0.9

Table S9: Results of the removal of the template ions after polymer synthesis. Each cycle was based on stirring the particles in a 3 M HNO_3 solution for 20 h. The supernatant was next analyzed by ICP-MS.

Polymer name		**D**		**V**		**M**		**DV**		**DM**	
Amount of Ba(II) in the removal solution and its percentage compared with the initial amount of Ba(II) used for the polymer synthesis		**n (mmol)**	**%**	**n (mmol)**	**%**	**n (mmol)**	**%**	**n (mmol)**	**%**	**n (mmol)**	**%**
IIP	**Cycle 1**	0.428	85.6	0.377	75.4	0.427	85.5	0.443	88.6	0.417	83.4
	Cycle 2	0.050	9.9	0.020	4.0	0.052	10.5	0.095	18.9	0.082	16.3
	Cycle 3	0.000	0.0	0.000	0.0	0.000	0.0	0.025	4.9	0.013	2.6
	TOTAL	0.478	**95.5**	0.397	**79.4**	0.480	**96.0**	0.562	**112.4**	0.512	**102.3**
NIP	**Cycle 1**	0.000		0.000		0.000		0.000		0.000	
	Cycle 2	0.000		0.000		0.000		0.000		0.000	
	Cycle 3	0.000		0.000		0.000		0.000		0.000	
	TOTAL	0.000		0.000		0.000		0.000		0.000	

Table S10: Uncertainty in relation with the absolute surface area in the sample holder according to the constructor.

Instrument	Tube size diameter (mm)	Gas	0.5 m^2	1 m^2	5 m^2	10 m^2	50 m^2	100 m^2
3Flex 3 ports	12	N_2	76%	38%	7.6%	3.8%	0.76%	0.38%
	12	Kr	3.1%	1.5%	0.31%	0.2%	0.03%	0.02%

Table S11: Summary of SPE procedures implemented on IIP/NIP V to try to improve the specificity, and observations made.

Mix 1: 15 µg L^{-1} of Ba(II), Sr(II), and Pb(II), and 10 µg L^{-1} of La(III), and Co(II).

Mix 2: 15 µg L^{-1} of Ba(II), Sr(II), and 10 µg L^{-1} of La(III), and Pb(II).

Each SPE procedure was performed once.

Aim of the trial	Conditioning step	Percolation step	Washing steps	Elution step	Results
Influence of Bis-Tris buffer and its concentration in the first washing step	3 mL of 25 mM Bis-Tris buffer at pH 7	Mix 1 in 25 mM Bis-Tris buffer at pH 7	W1: 0.5 mL of 25 mM (or 100 mM or 200 mM) Bis-Tris buffer at pH 7 W2: 0.5 mL HNO_3 pH 4	E1: 0.5 mL HNO_3 pH 3 E2: 0.5 mL HNO_3 pH 2 E3: 3 mL HNO_3 0.5 M	Elements (including Ba(II)) co-extracted: -For 25 mM: in fractions E1 (10%) and E2 (80% and more) → results comparable with those observed when W1 is 0.5 mL of UP water. -For 100 mM: in fractions E1 (40%) and E2 (60%). -For 200 mM: in fractions E1 (30%) and E2 (70%).
Influence of pH			W1: 0.5 mL of UP water W2: 0.5 mL HNO_3 pH 3.5	E1: 0.5 mL HNO_3 pH 3 E2: 0.5 mL HNO_3 pH 2.5 E3: 0.5 mL HNO_3 pH 2 E4: 3 mL HNO_3 0.5 M	Elements (including Ba(II)) co-extracted in fractions E1 (60-70%) and E2 (20-30%).
			W: 0.5 mL HNO_3 pH 3.3	E1: 0.5 mL HNO_3 pH 3.1 E2: 0.5 mL HNO_3 pH 2.5 E3: 3 mL HNO_3 0.5 M	Elements (including Ba(II)) co-extracted in fractions E1 (30-40%) and E2 (60%).
Influence of percolation medium, and of pH	3 mL of HNO_3 pH 4	Mix 2 in 1 mL HNO_3 pH 4	W: 0.5 mL HNO_3 pH 4	E1: 0.5 mL HNO_3 pH 3.5 E2: 0.5 mL HNO_3 pH 3 E3: 0.5 mL HNO_3 pH 2.5 E4: 0.5 mL HNO_3 pH 2 E5: 3 mL HNO_3 0.5 M	No retention for Ba(II), Sr(II), and La(III) at pH 4 (70-80% in fraction P). Pb(II) is eluted in fraction E1 (90%).
Influence of volume of washing solution	3 mL of 25 mM Bis-Tris buffer at pH 7	Mix 2 in 25 mM Bis-Tris buffer at pH 7	W: 0.5 mL of UP water	E1 to E10: 10 x 1 mL HNO_3 pH 4 E11: 3 mL HNO_3 0.5 M	Ba(II), Sr(II), and La(III) co-extracted in fraction E3 (70-80%). Pb(II) begins to be eluted in E3 (30%) and continues until E11 (first mL).
	3 mL of HNO_3 pH 6	Mix 2 in 1 mL HNO_3 pH 6	W: 0.5 mL of UP water	E1 to E10 : 10 x 0.5 mL HNO_3 pH 4 E11: 3 mL HNO_3 0.5 M	Ba(II), and Sr(II) co-extracted in fraction E1 (20%) and in E2 (70%). La(III) begins to be eluted in E2 (40%) and continues until E11. Pb(II) begins to be eluted in fraction E6 but 70% falls into E11.

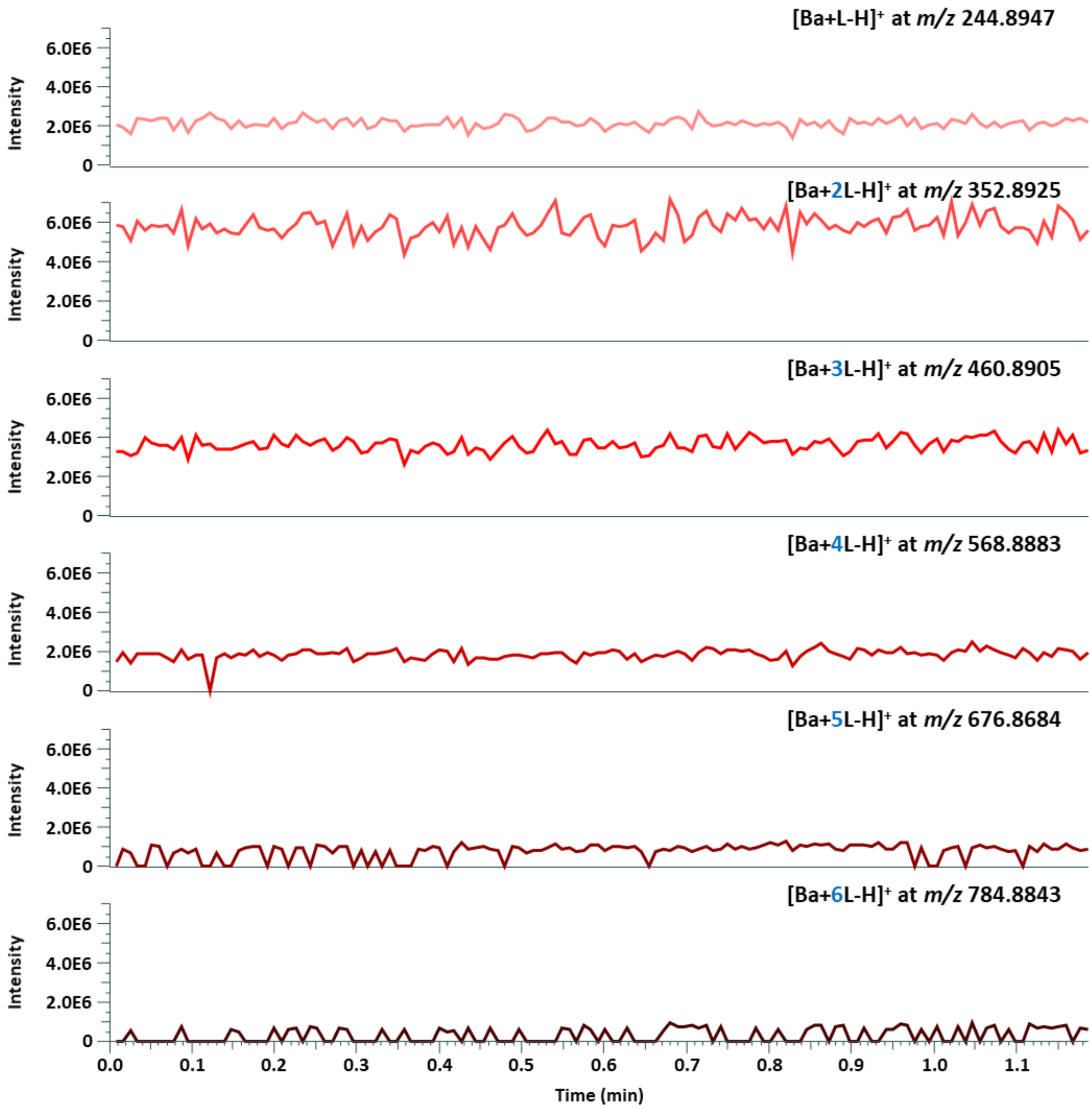

Figure S1: EICs of complexes in the form $[Ba+nL-H]^+$, n ϵ {1, 2, 3, 4, 5, 6}, after infusion of a mixture of barium nitrate and VPA as ligand (L) with a molar ratio of 1/6 ($[Ba^{2+}]=10^{-4}$ M) after 24 h of complexation.

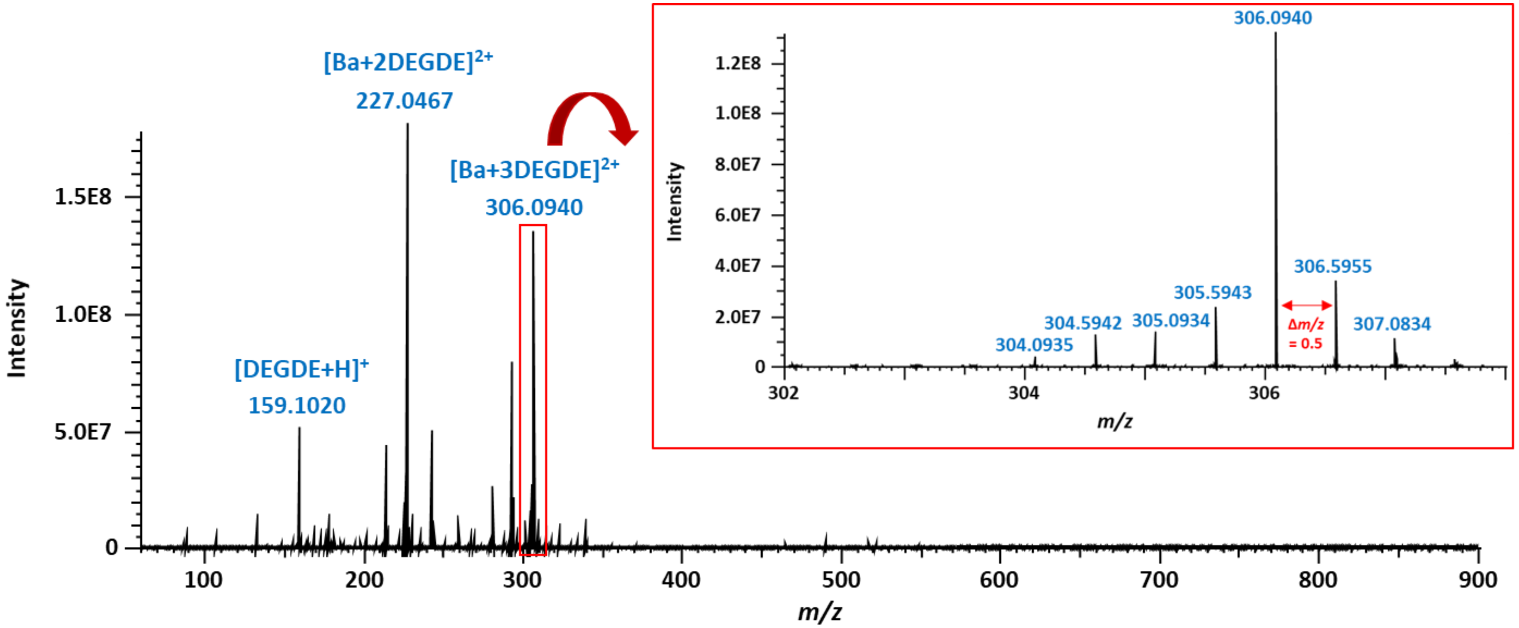

Figure S2: Average mass spectrum (*m/z* 60–900) for a mixture of barium nitrate and DEGDE with a molar ratio of 1/6 ($[Ba^{2+}]=10^{-4}$ M) after 24 h of complexation.

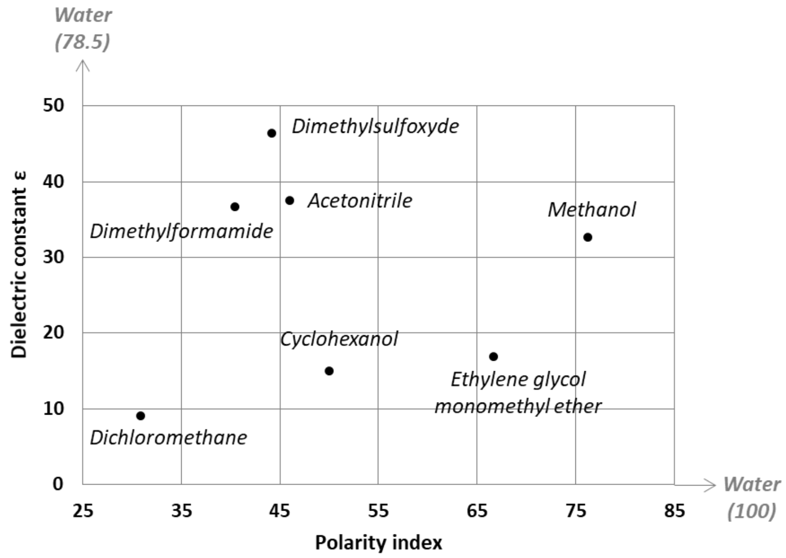

Figure S3: Mapping of solvents usually employed for MIP and IIP synthesis according to their polar and dissociative character. Data extracted from [1].

---

[1] I.M. Smallwood, Handbook of organic solvent properties, Arnold; Halsted Press, London: New York, 1996.

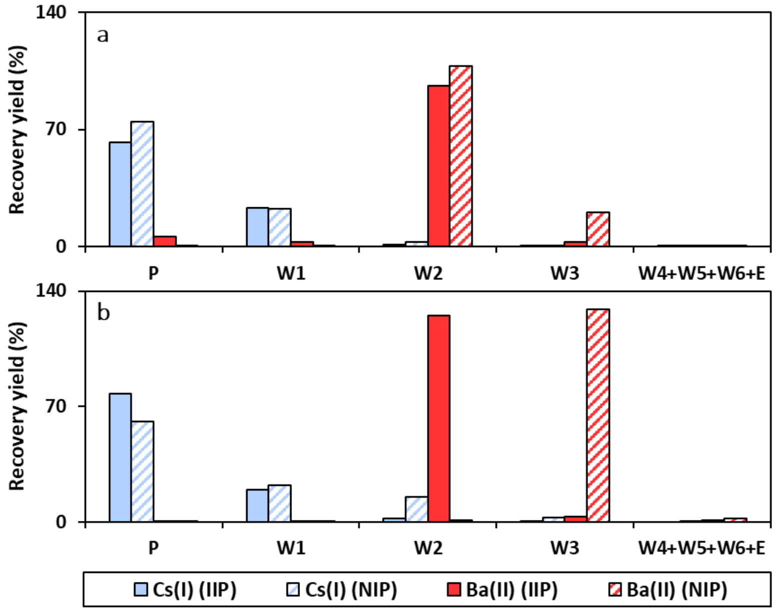

Figure S4: Influence of a fine decrease in the pH from 3 to 2 of the washing solutions on SPE profiles of Cs(I) and Ba(II) obtained on IIPs and NIPs DV (a) and DM (b). P: percolation of 1 mL of NH_3 solution adjusted to pH 10 and spiked with 25 µg L^{-1} of Cs(I) and Ba(II). W1 to W6: washing with 0.5 mL of HNO_3 pH 3, 0.5 mL of HNO_3 pH 2.8, 0.5 mL of HNO_3 pH 2.6, 0.5 mL of HNO_3 pH 2.4, 0.5 mL of HNO_3 pH 2.2, and 0.5 mL of HNO_3 pH 2, respectively. E: Elution with 3 mL of HNO_3 0.5 M. All fractions were analyzed with an ICP-(CC)-Q-MS system (Agilent 7700x).The presented data ensue from one SPE.

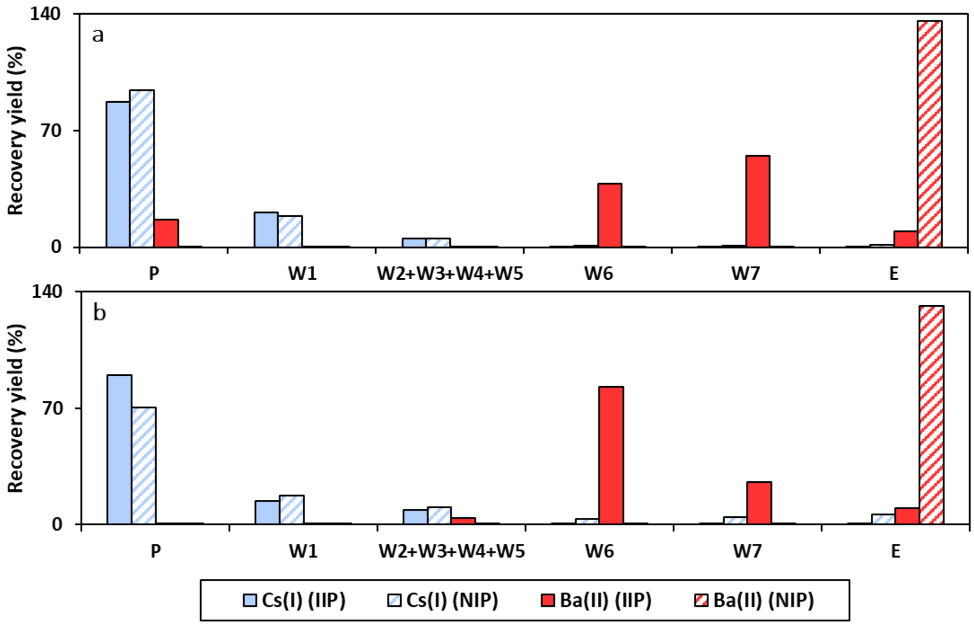

Figure S5: Effect of an ethanol gradient during the washing steps on SPE profiles of Cs(I) and Ba(II) obtained on IIPs and NIPs DV (a) and DM (b). P: percolation of 1 mL of NH_3 solution adjusted to pH 10 and spiked with 25 µg L^{-1} of Cs(I) and Ba(II). W1 to W7: washing with 0.5 mL of UP water, 0.5 mL of HNO_3 pH 4, 0.5 mL of HNO_3 pH 4/EtOH (95/5, v/v), 0.5 mL of HNO_3 pH 4/EtOH (90/10, v/v), 0.5 mL of HNO_3 pH 4/EtOH (80/20, v/v), 0.5 mL of HNO_3 pH 4/EtOH (70/30, v/v), and 0.5 mL of HNO_3 pH 4/EtOH (60/40, v/v), respectively. E: Elution with 3 mL of HNO_3 0.5 M. All fractions were analyzed with an ICP-(CC)-Q-MS system (Agilent 7700x). Tl (*m/z* 205 monitored) at 0.1 µg L^{-1} was used as internal standard to correct matrix effects in solutions containing EtOH. The presented data ensue from one SPE.

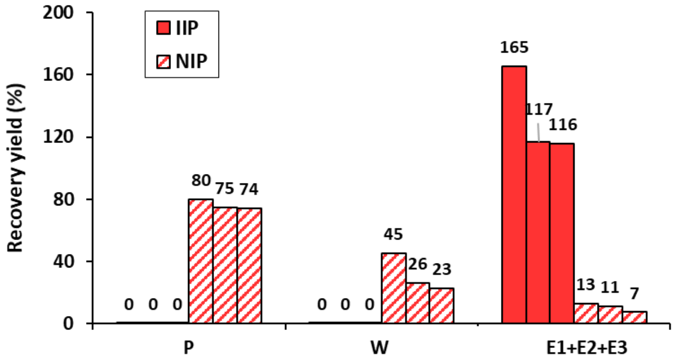

Figure S6: Three repetitions of the extraction of Ba(II) on IIP and NIP V. P: percolation of 1 mL of 25 mM Bis-Tris buffer at pH 7 spiked with 25 µg L^{-1} of Ba(II). W: washing with 0.5 mL of UP water and 0.5 mL of HNO_3 pH 4. E1 to E3: Elution with 0.5 mL of HNO_3 pH 3, 0.5 mL of HNO_3 pH 2, and 3 mL of HNO_3 0.5 M, respectively. All fractions were analyzed with an ICP-(CC)-Q-MS system (Agilent 7700x).

Thermogravimetric analyses

The thermal stability of the polymers was investigated by TGA. The objective was to evaluate until which temperature it was possible to heat samples during the degassing phase that precedes a BET analysis. TGA curves in Figure S7 exhibit a slope change from 300°C, followed by a large loss of mass which can be attributed to polymer decomposition. In addition, the three curves show similar degradation pattern, meaning neither the nature of the monomers used for syntheses (IIP V *versus* IIP DV), nor the polymer structure arising from the presence or absence of template ions (IIP V *versus* NIP V) has an impact on the degradation temperature. This parameter seems to be imposed by the main matrix components, namely the co-monomer and the cross-linker which are present in larger proportions.

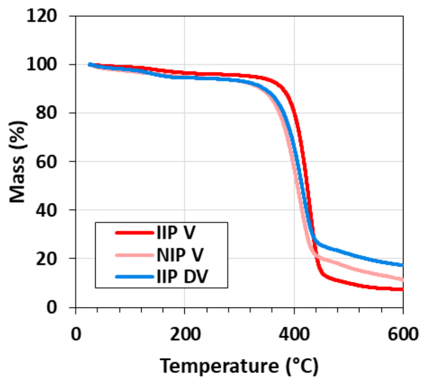

Figure S7: Thermogravimetric analyses of IIP V and its NIP, and IIP DV.

BET experiments

The desorption isotherm of the most promising IIP, namely V, falls below the adsorption isotherm due to the low amount of nitrogen adsorbed (Figure S8a). Indeed, the absolute surface value measured for this polymer (0.6 m^2) is well below the range recommended by the constructor (10 to 100 m^2 to have an uncertainty of less than 5%), thus leading to large uncertainties (~76% according to the instrument specifications) on the produced results (Table S10). To sufficiently reduce uncertainties, we could have increased the initial sample mass by a factor of 10 to 20 but such a mass was not available after realizing the post-synthesis steps. An alternative option could be to replace N_2 with Kr, the recommended gas for materials of low specific surface areas. Using the same amount of sample, uncertainties could be reduced to 3% due to the fact that Kr is monoatomic (N_2 is diatomic and its electronic cloud can be distorted resulting in different orientations and contact areas with the studied material) and has a lower saturation vapor pressure than N_2 (267 Pa against 101 kPa at -77 K).

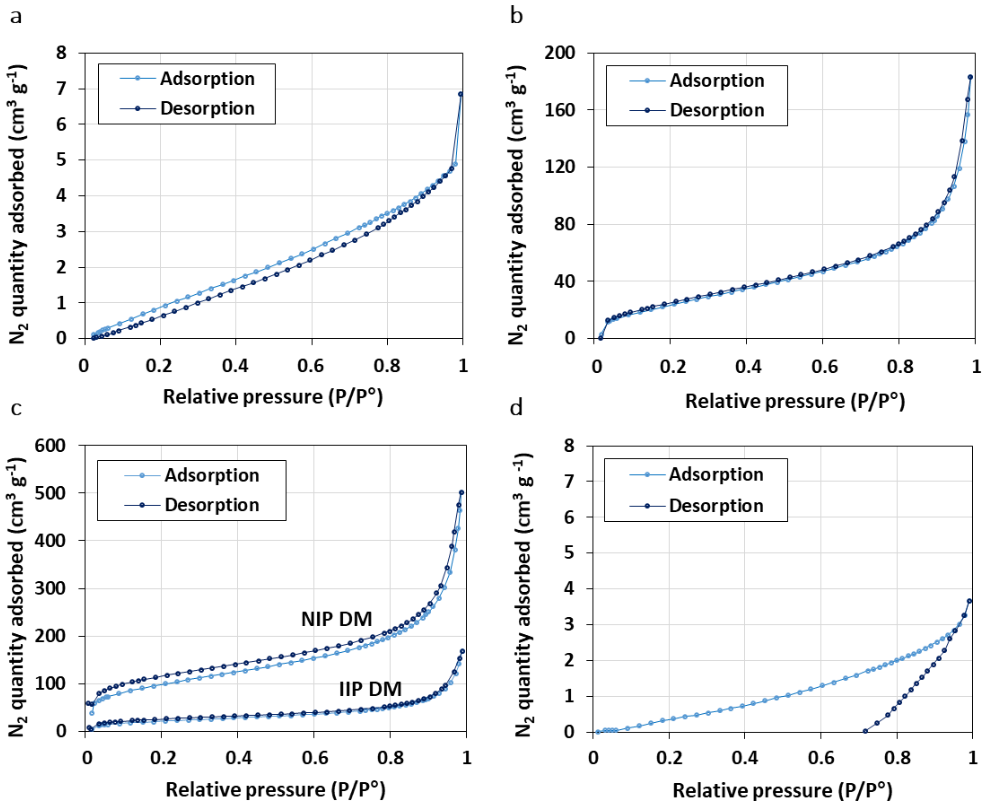

Figure S8: N_2 adsorption/desorption isotherms of IIP V (a), NIP V (b), IIP/NIP DM (c), and IIP Ni (d).

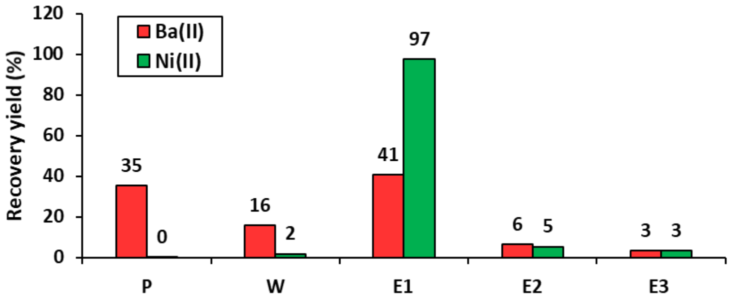

Figure S9: SPE profiles of Ba(I) and Ni(II) obtained on IIP Ni. P: percolation of 1 mL of 25 mM Bis-Tris buffer at pH 7 spiked with 25 µg L^{-1} of Ba(II) and Ni(II). W: washing with 0.5 mL of UP water and 0.5 mL of HNO_3 pH 4. E: Elution with 0.5 mL of HNO_3 pH 3, 0.5 mL of HNO_3 pH 2, and 3 mL of HNO_3 0.5 M, respectively. All fractions were analyzed with an ICP-QQQ-MS (Agilent 8800) monitoring ^{61}Ni and ^{137}Ba. The presented data ensue from one SPE.

Polyatomic interferences on our measurement system

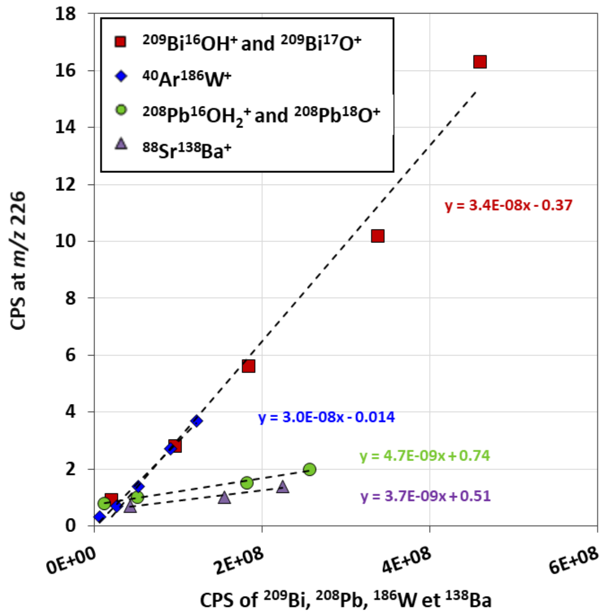

Figure S10: Polyatomic interferences of Bi, Ar, Pb, and Ba/Sr (weight ratio 1/1) at *m/z* 226. Solutions with concentrations ranging between 10 and 230 µg L^{-1} were analyzed with a desolvating nebulizer (Apex Omega) as introduction system coupled to an ICP-QQQ-MS (Agilent 8800).

In order to identify which of the two Bi and Pb species contribute the most to the signal at *m/z* 226, we also measured signals at *m/z* 224 ($^{208}Pb^{16}O^+$) and 225 ($^{209}Bi^{16}O^+$) and used the oxygen natural isotope abundance to determine the contribution of $^{208}Pb^{18}O^+$ and $^{209}Bi^{17}O^+$ to the measured signal at *m/z* 226 (Eq. (3) and (4)).

$$S_{Pb^{18}O} = S_{Pb^{16}O} \times \frac{A_{^{18}O}}{A_{^{16}O}} \qquad \text{Eq. (3)}$$

$$S_{Bi^{17}O} = S_{Bi^{16}O} \times \frac{A_{^{17}O}}{A_{^{16}O}} \qquad \text{Eq. (4)}$$

where $S_{Pb^{18}O}$ and $S_{Bi^{17}O}$ are the calculated signals at *m/z* 226 (cps), $S_{Pb^{16}O}$ and $S_{Bi^{16}O}$ are the measured signals at *m/z* 224 and 225 respectively (cps), and $A_{^{18}O}$, $A_{^{17}O}$, and $A_{^{16}O}$ are the oxygen natural abundances for ^{18}O, ^{17}O, and ^{16}O.

We found out that 96.0% and 99.5% of the measured signals were due to $^{208}Pb^{16}O^1H_2^+$ and $^{209}Bi^{16}O^1H^+$, respectively, even though these are interferences involving four and three atoms.